

Recent progress in nickelate superconductors

Yuxin Wang,^{1,2} Kun Jiang,^{1,2,*} Jianjun Ying,^{3,4} Tao Wu,^{3,4,†} Jinguang Cheng,^{1,2} Jiangping Hu,^{1,5,6,‡} and Xianhui Chen^{3,4,§}

¹Beijing National Laboratory for Condensed Matter Physics and Institute of Physics, Chinese Academy of Sciences, Beijing 100190, China

²School of Physical Sciences, University of Chinese Academy of Sciences, Beijing 100190, China

³Hefei National Laboratory for Physical Sciences at the Microscale,

University of Science and Technology of China, Hefei, Anhui 230026, China

⁴CAS Key Laboratory of Strongly-coupled Quantum Matter Physics, Department of Physics,

University of Science and Technology of China, Hefei, Anhui 230026, China

⁵Kavli Institute of Theoretical Sciences, University of Chinese Academy of Sciences, Beijing, 100190, China

⁶New Cornerstone Science Laboratory, Beijing, 100190, China

(Dated: September 11, 2025)

The discovery of superconductivity in nickelate compounds has opened new avenues in the study of high-temperature superconductors. Here we provide a comprehensive overview of recent progress in the field, including all different nickelate systems, reduced-Ruddlesden-Popper-type infinite layer LaNiO_2 , Ruddlesden-Popper-type bilayer $\text{La}_3\text{Ni}_2\text{O}_7$ and trilayer $\text{La}_4\text{Ni}_3\text{O}_{10}$. We begin by introducing the superconducting properties of the hole-doped LaNiO_2 system, which marked the starting point for nickelate superconductivity. We then turn to the bilayer $\text{La}_3\text{Ni}_2\text{O}_7$ system, discussing both its high-pressure and thin-film superconducting phases. This is followed by an examination of the trilayer $\text{La}_4\text{Ni}_3\text{O}_{10}$ system and other related multilayer nickelates. Throughout the review, we highlight emerging trends, key challenges, and open questions. We conclude by addressing current limitations in materials synthesis and characterization, and future directions that may help uncover the mechanisms driving superconductivity in these complex oxide systems.

I. INTRODUCTION

The discovery of superconductivity in copper oxides in 1986 opened a new frontier in the quest for high-temperature—and potentially even room-temperature—superconductors [1–3]. These materials marked not only a major step toward real-world applications but also unveiled a rich landscape of exotic quantum phenomena. In high-temperature (high- T_c) superconductors, electrons interact strongly in ways that defy the conventional Bardeen-Cooper-Schrieffer (BCS) theory, revealing complex behaviors driven by electronic correlations. Their ability to sustain superconductivity within layered structures containing intertwined magnetic and electronic orders sparked a wave of research into unconventional pairing mechanisms. The discovery of iron-based superconductors in 2008 further broadened the family of high- T_c materials [4–6]. Yet, despite decades of intense investigation, the underlying mechanisms that drive high-temperature superconductivity remain one of the most profound and enduring mysteries in modern condensed matter physics. One promising approach to better understand unconventional pairing is to explore and identify more high- T_c superconductors.

Nickel, as the nearest neighbor of copper on the periodic table of elements, has long been considered a promising candidate for hosting high-temperature superconductivity since early 1990s. Notably, Maurice Rice and collaborators proposed that superconductivity could emerge in doped LaNiO_2 , given that Ni^+ shares the same $3d^9$ valence electron configu-

ration as Cu^{2+} in cuprate superconductors [7, 8]. After more than three decades of exploration, this prediction was finally realized with the discovery of superconductivity in nickelates [9], marking the beginning of the “nickel age” of superconductivity [10, 11]. Recently, the family of nickelate superconductors has grown rapidly, now including compounds such as $\text{La}_3\text{Ni}_2\text{O}_7$ [12, 13], $\text{La}_4\text{Ni}_3\text{O}_{10}$ [14–16], and other related materials [17, 18]. These discoveries have introduced a new and exciting chapter in the study of high- T_c superconductors. The purpose of this paper is to review the recent advances in nickelate superconductors and to provide an accessible introduction to this rapidly evolving field.

From the valence electron perspective, the electron distribution of free Ni atom can be formally written as $[\text{Ar}]3d^84s^2$ or $[\text{Ar}]3d^94s^1$. The most common oxidation state of Nickel is Ni^{2+} while the ionic charge of Ni oxides ranges from 1+ to 3+, as plotted in Fig. 1. As mentioned above, Ni^{1+} has $3d^9$ valence electrons while Ni^{2+} , Ni^{3+} belong to $3d^8$ or $3d^7$ respectively. We want to add one caveat that for ionic charge larger than 2 state Ni^{2+} , the extra holes are always doped to oxygen as Zhang-Rice singlets in cuprates [19], where the oxygen p orbital is also important [20].

From a structural perspective, nickelate superconductors belong to the well-known Ruddlesden-Popper (RP) family of perovskite structures [21]. The general chemical formula for an RP phase is $A_{n+1}\text{Ni}_n\text{O}_{3n+1}$, where A is a cation and n denotes the number of perovskite layers. For clarity, we consider the case with lanthanum (La) as the A -site ion, as illustrated in Fig. 1. RP phases consist of multiple perovskite-like LaNiO_3 layers interleaved by single rock-salt-type LaO layers. For $n = 1$, the resulting structure is La_2NiO_4 , where nickel exists in a 2+ oxidation state. Increasing to $n = 2$ yields the bilayer compound $\text{La}_3\text{Ni}_2\text{O}_7$, and $n = 3$ gives the trilayer $\text{La}_4\text{Ni}_3\text{O}_{10}$. The corresponding average nickel oxidation states are 2.5+ and 2.67+, respectively. In the limit

* jiangkun@iphy.ac.cn

† wutao@ustc.edu.cn

‡ jphu@iphy.ac.cn

§ chenxh@ustc.edu.cn

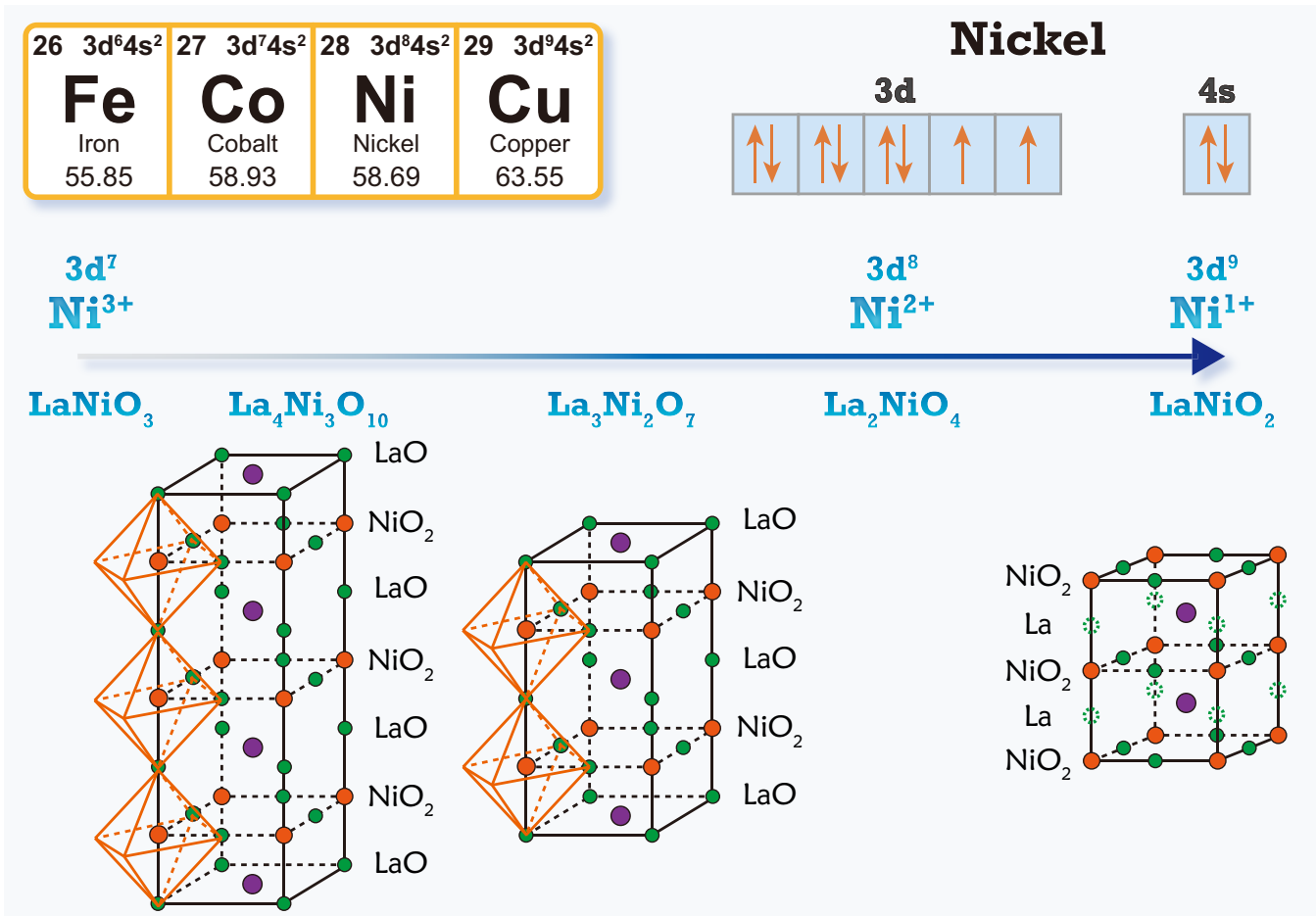


FIG. 1. Structures, Ionic Charges, and Valence States of Nickelates. Ni atom has electron configuration $[\text{Ar}] 3d^8 4s^2$ or $[\text{Ar}] 3d^9 4s^1$. In nickel oxides, the Ni ionic charge typically ranges from +1 to +3 and the most common oxidation state is Ni^{2+} . The RP nickelates phases $\text{La}_{n+1}\text{Ni}_n\text{O}_{3n+1}$ have ionic charges between Ni^{2+} and Ni^{3+} . The bilayer compound $\text{La}_3\text{Ni}_2\text{O}_7$ and the trilayer $\text{La}_4\text{Ni}_3\text{O}_{10}$ have recently been identified as superconductors. A reduced RP phase, LaNiO_2 , can be obtained from the RP LaNiO_3 through chemical reduction. These removed oxygen sites are indicated by dashed green circles in LaNiO_2 . Hole-doped LaNiO_2 is the first nickelate superconductor.

$n \rightarrow \infty$, the structure converges to the compound LaNiO_3 , in which nickel has a 3+ oxidation state. Thus, the valence state of nickel across the RP nickelates spans from Ni^{2+} and Ni^{3+} . To achieve a Ni d^9 electronic configuration, analogous to that of Cu^{2+} in cuprates, one can remove an oxygen atom from LaNiO_3 , yielding the reduced-RP LaNiO_2 . The synthesis of RP nickelates has been studied extensively for decades [22–29]. Among these, La_2NiO_4 and LaNiO_3 are the most stable and well-characterized phases, while $\text{La}_4\text{Ni}_3\text{O}_{10}$ and $\text{La}_3\text{Ni}_2\text{O}_7$ are more challenging to synthesize.

We want to organize this paper as follows: we begin with a brief overview of superconductivity in the hole-doped LaNiO_2 system (we will label it as the 112 system for short). We then focus on the bilayer $\text{La}_3\text{Ni}_2\text{O}_7$ (short for 327 system), highlighting both the high-pressure and thin-film superconducting phases. Following this, we examine the trilayer $\text{La}_4\text{Ni}_3\text{O}_{10}$ (short for 43(10) system) and other relative multilayer nickelates. Finally, we discuss current limitations in the field and outline future directions for research.

Before delving into detailed discussions, we would like

to highlight an important point. Although multilayer nickelates exhibit superconductivity, they are fundamentally different from their cuprate counterparts. In multilayer cuprates, superconductivity primarily resides within individual CuO_2 planes, which are only weakly coupled. In contrast, the layers in multilayer nickelates are strongly coupled, indicating that superconductivity arises collectively in the multilayers.

II. 112

Since several comprehensive reviews on LaNiO_2 -based superconductors already exist [30, 31], we provide only a brief overview here. As discussed earlier, Ni^{1+} is both rare and thermodynamically unstable. The typical approach to stabilize it involves removing oxygen from the more stable LaNiO_3 , as illustrated in Fig. 2(a). This reduction is commonly achieved via a soft-chemistry topotactic reaction using metal hydrides, a method applied to LaNiO_2 since 1999 [32–35]. A major breakthrough came in 2019, when Li et

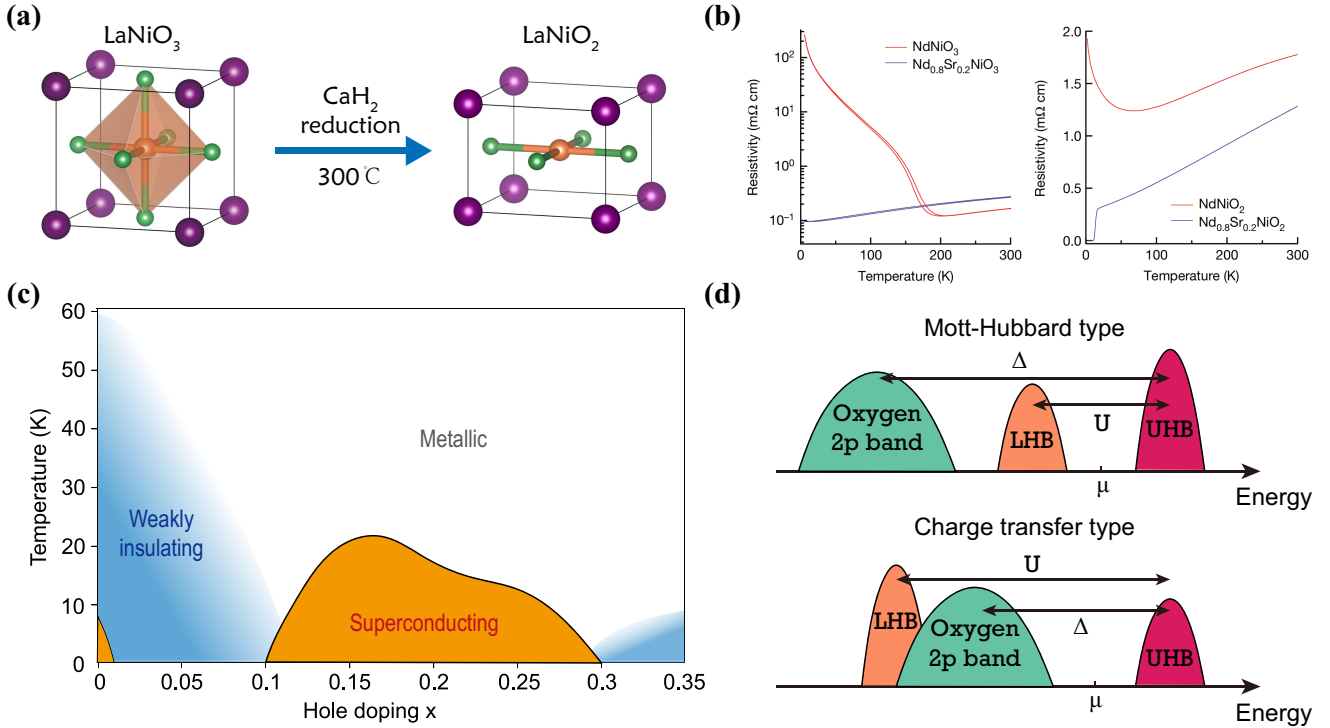


FIG. 2. (a) LaNiO₂ is synthesized by reducing LaNiO₃ using CaH₂, which selectively removes oxygen atoms from the LaO planes [9]. (b) The left panel shows the resistivity of NdNiO₃ (insulating) and Nd_{0.8}Sr_{0.2}NiO₃ (metallic) thin films. The right panel displays the resistivity of the reduced compounds, NdNiO₂ and Nd_{0.8}Sr_{0.2}NiO₂. A superconducting transition with an onset at 14.9 K is observed in Nd_{0.8}Sr_{0.2}NiO₂ [9]. (c) The global phase diagram of hole-doped LaNiO₂ [30]. (d) The “parent” state of LaNiO₂ is a Mott insulator, in contrast to cuprates, where the parent state is a charge-transfer insulator. We emphasize that the “parent” state here refers to the idealized insulating limit of LaNiO₂, which may differ from the actual, experimentally realized parent compound.

al. successfully synthesized hole-doped Nd_{0.8}Sr_{0.2}NiO₂ superconducting thin films on SrTiO₃ substrates using CaH₂ as the reducing agent [9]. As shown in Fig. 2(b), the parent NdNiO₃ (a low-temperature-magnetic insulator) and the metallic Nd_{0.8}Sr_{0.2}NiO₃ films were first grown using pulsed-laser deposition. Subsequent reduction with CaH₂ yielded NdNiO₂, which exhibits a resistivity upturn below 70 K. In contrast, the hole-doped Nd_{0.8}Sr_{0.2}NiO₂ enters a superconducting state below 14.9 K.

After six years of intensive research, a clearer picture of the hole-doped 112 phase diagram has emerged, as shown in Fig. 2(c). Similar to the cuprates, a superconducting dome appears in the doping range of approximately $x = 0.1$ to $x = 0.3$, with the superconducting transition temperature T_c reaching up to 40 K [36, 37]. This superconducting dome is flanked on both sides by weakly insulating phases, characterized by a low-temperature resistivity upturn—consistent with the behavior observed in undoped NdNiO₂, shown in Fig. 2(b). Interestingly, the $x = 0$ composition is not always insulating. Several studies have reported a new superconducting phase at $x = 0$ [38–40], as highlighted in Fig. 4(a).

Although Ni¹⁺ shares the same d^9 electronic configuration as Cu²⁺ in the cuprates, hole-doped LaNiO₂ differs from hole-doped cuprates in the following respects:

1. The ideal insulating limit, or the “parent” state, LaNiO₂

is considered a Mott insulator rather than a charge-transfer insulator [41, 42]. As illustrated in Fig. 2(d), in cuprate superconductors, the Cu d -orbitals split into a lower Hubbard band (LHB) and an upper Hubbard band (UHB), separated by the on-site Coulomb interaction energy U . The oxygen p band lies between these two Hubbard bands, with a charge-transfer gap Δ_{CT} between the O p levels and the UHB. As a result, doped holes in cuprates tend to reside on oxygen sites, forming the well-known Zhang-Rice singlet state [19]. In contrast, for LaNiO₂, the charge-transfer gap Δ_{CT} is significantly larger than the Hubbard U , which pushes the oxygen p band below the LHB. Consequently, doped holes in LaNiO₂ preferentially occupy Ni d orbitals rather than oxygen sites. This key distinction suggests that hole-doped LaNiO₂ may behave more like electron-doped cuprates rather than hole-doped ones.

2. The electronic structure of LaNiO₂ exhibits pronounced k_z dispersion. Thanks to advances in sample quality, angle-resolved photoemission spectroscopy (ARPES) measurements on hole-doped LaNiO₂ have become feasible [43, 44]. For instance, in La_{0.8}Sr_{0.2}NiO₂ (LSNO), the low-energy electronic states are primarily derived from Ni $3d_{x^2-y^2}$ and La $5d$ orbitals, as shown in Fig. 3(a). The Fermi surface (FS) contour

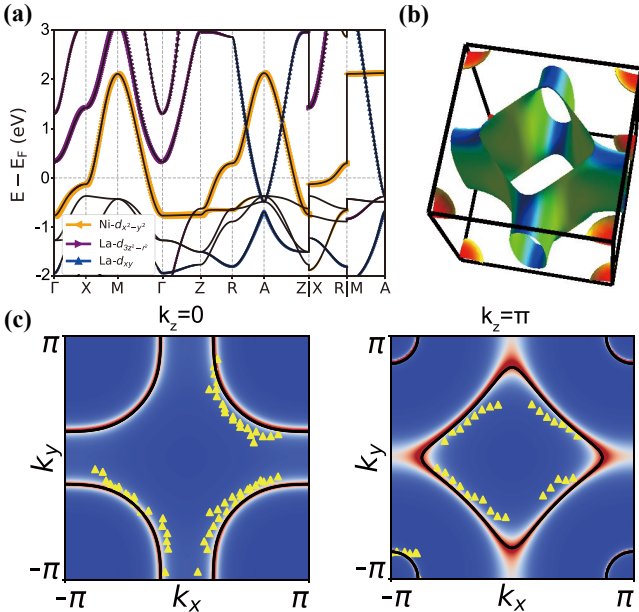


FIG. 3. (a) The band structure of LaNiO_2 , where the dominate valence electrons are from $\text{Ni } 3d_{x^2-y^2}$ and $\text{La } 5d$ orbitals. (b) The three-dimensional Fermi surface contour of $\text{La}_{0.8}\text{Sr}_{0.2}\text{NiO}_2$. (c) The Fermi surfaces at $k_z = 0$ and $k_z = \pi$ calculated using tight-binding and dynamical mean-field theory [45]. The yellow markers indicate ARPES experimental data points [43].

at $k_z = 0$, plotted in Figs. 3(b-c), reveals a hole-like FS from the $\text{Ni } 3d_{x^2-y^2}$ orbital, closely resembling that of cuprates. However, this hole FS transforms into an electron-like FS at $k_z = \pi$, highlighting the strong three-dimensionality of the system. Since reduced dimensionality is believed to be a key factor contributing to the high T_c in cuprates, the pronounced k_z dispersion in LSNO may be one reason why its superconducting transition temperature remains lower in comparison [45].

3. The role of $5d$ electrons in LaNiO_2 remains a topic of ongoing debate. In addition to the Fermi surface derived from $\text{Ni } 3d$ electrons, ARPES measurements reveal a small Fermi pocket near the corner of the Brillouin zone (BZ), attributed to $\text{La } 5d$ electrons [43, 44]. Notably, the $5d$ band shows no observable band renormalization, indicating that electronic correlations in this band are very weak. This weak correlation is consistent with expectations based on doping and band structure. Density functional theory (DFT) calculations show that the $5d$ band has a large bandwidth of approximately 2 eV, and the observed Fermi pocket lies far from half-filling. As a result, the primary role of these weakly correlated $5d$ electrons is to provide intrinsic hole doping to the $\text{Ni } 3d$ band. Consequently, LaNiO_2 is not a true parent compound in the sense of having a half-filled $3d$ band, due to this self-doping effect from the $5d$ states.

From Fig. 2(c) phase diagram, there are two regions of weak insulator with a resistivity upturn. The origin of this upturn is widely debated. There are two major scenarios:

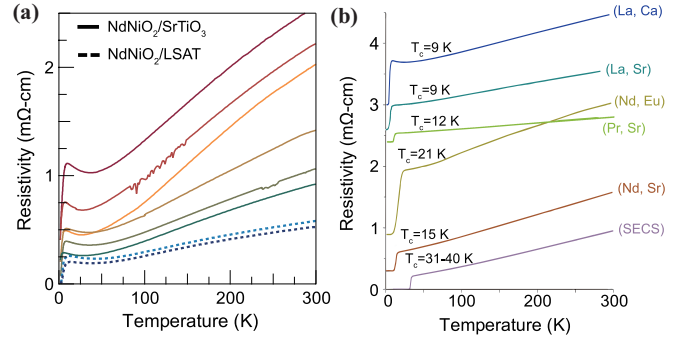


FIG. 4. (a) Superconducting transition found in different NdNiO_2 samples [38]. (b) In comparison to other 112 SCs, $\text{Sm}_{1-x}\text{Sr}_x\text{NiO}_2$ co-doped with Eu and Ca (SECS) achieve higher transition temperatures, reaching up to $T_c \sim 40$ K [36].

Kondo scattering and the disorder effect. Theoretically, it was proposed that the $5d$ electron contributes to conductivity, which is Kondo-scattered by the localized $\text{Ni } 3d$ electrons at low temperature [46]. On the other hand, one should notice that topotactic reduction always introduces various defects to LaNiO_2 . This kind of disorder effect is unavoidable for the 112 system. It has been shown that by improving sample quality, the upturn behavior shows a clear dependence on the disorder level in the overdoped region [47].

Finally, we highlight two recent advances in the 112 nickelate systems:

- Superconductivity at $x = 0$: In a study conducted a few years ago, signs of superconductivity were already observed in undoped LaNiO_2 [48]. Recently, superconductivity with $T_c \approx 11$ K has been definitively observed in the nominally undoped “parent” compounds NdNiO_2 and PrNiO_2 [38–40], adding a new feature to the 112 phase diagram. As shown in Fig. 4(a), improvements in substrate selection and sample quality for NdNiO_2 have led to significantly reduced residual resistivity. While some samples still display resistivity upturns, superconducting transitions are clearly observed. This finding underscores the crucial role of disorder in determining the physical properties of 112 systems. It also raises important questions: Is the $x = 0$ superconductivity intrinsic? How is it connected to the main superconducting dome?
- Enhancement of T_c via chemical tuning: Raising T_c remains a key goal in 112 research. Carrier doping and epitaxial strain from substrates are known to significantly influence superconductivity in thin films. Recently, $\text{Sm}_{1-x}\text{Sr}_x\text{NiO}_2$ and co-doped variants incorporating Eu and Ca have achieved transition temperatures approaching 40 K [36, 37], as shown in Fig. 4(b). These co-doped compounds exhibit remarkably low resistivity—on the order of 0.01 m $\Omega \cdot \text{cm}$ —and a record-small c -axis lattice parameter. The origin of this improvement remains unclear, calling for further experimental and theoretical investigation.

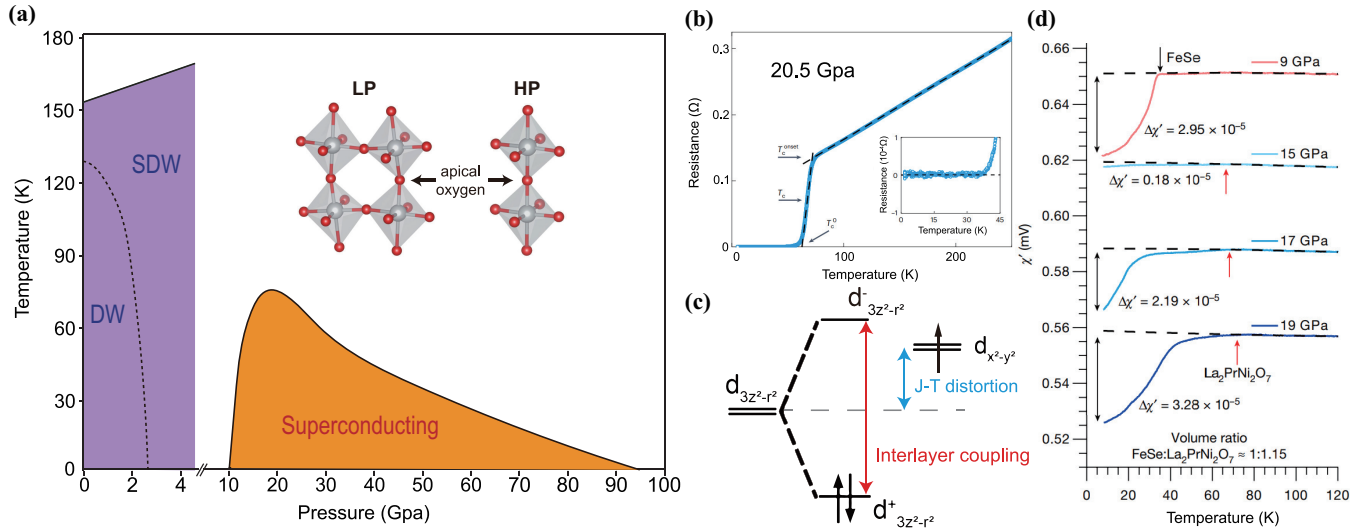


FIG. 5. (a) Global phase diagram of $\text{La}_3\text{Ni}_2\text{O}_7$ as a function of pressure and temperature, revealing a transition from a low-pressure (LP) phase to a high-pressure (HP) phase. The inset illustrates the distinct crystal structures associated with each phase. The apical oxygen, which connects the two NiO_2 layers, plays a key role in the electronic properties of the 327 compound. (b) Temperature-dependent resistance $R(T)$ of $\text{La}_3\text{Ni}_2\text{O}_7$ at 20.5 GPa, showing a superconducting transition onset at 66 K and reaching zero resistance around 40 K [49]. (c) Schematic of the e_g orbital energy levels in bilayer $\text{La}_3\text{Ni}_2\text{O}_7$. Due to Jahn-Teller (J-T) distortion, the $d_{3z^2-r^2}$ orbital lies below the $d_{x^2-y^2}$ orbital. Strong interlayer coupling further splits the $d_{3z^2-r^2}$ states into bonding ($d_{3z^2-r^2}^+$) and antibonding ($d_{3z^2-r^2}^-$) orbitals. (d) The a.c. magnetic susceptibility $\chi'(T)$ of $\text{La}_2\text{PrNi}_3\text{O}_7$ under various pressures of up to 19 GPa. The dashed line represents the background extrapolated from the high-temperature region [13]. The superconducting shielding volume fraction can reach more than 90%.

In summary, the 112 nickelates represent a new class of superconductors based on the $3d^9$ configuration, analogous to hole-doped cuprates. While $5d$ electrons introduce additional complexity, the low-energy physics is still primarily governed by the Ni $3d_{x^2-y^2}$ orbitals. Despite some notable differences, many key concepts from cuprate superconductivity are transferable to the 112 systems. In particular, the widely anticipated nodal d -wave pairing symmetry remains a central prediction awaiting experimental confirmations [50–54].

III. 327

Following the discovery of superconductivity in hole-doped $3d^9$ 112 nickelates, pressurized $\text{La}_3\text{Ni}_2\text{O}_7$ was identified in 2023 as a superconductor with an onset T_c near 80 K [12]. The compound 327 has been successfully synthesized for several decades [25–28]. As highlighted in Fig. 1, $\text{La}_3\text{Ni}_2\text{O}_7$ possesses a distinct valence electron configuration of $3d^{7.5}$, differing from the $3d^9$ configuration of the 112 nickelates. This establishes $\text{La}_3\text{Ni}_2\text{O}_7$ as a novel class of nickelate superconductor. While a previous review details the early development of $\text{La}_3\text{Ni}_2\text{O}_7$ properties [55], this work aims to describe the system from a different perspective. Readers seeking information on its history, synthesis, and other aspects are directed to Ref. [55]. We also want to note that owing to the crystal quality of $\text{La}_3\text{Ni}_2\text{O}_7$ or polycrystalline sample forms, different references may arrive at different conclusions.

A. Phase diagram and high-pressure superconductivity

The global phase diagram as function of pressure and temperature is plotted in Fig. 5 (a). The phase diagram contains two parts: the low-pressure (LP) region and the high-pressure (HP) region. The major difference between the LP phase and the HP phase comes from their structure. As described in Fig. 1, the central ingredient of $\text{La}_3\text{Ni}_2\text{O}_7$ structure is the bilayer NiO_2 planes. Each bilayer is formed by two shared apical oxygen NiO_6 octahedra. This shared apical oxygen has great importance in the physical properties of $\text{La}_3\text{Ni}_2\text{O}_7$. In the HP phase, two NiO_6 octahedra are lined up, making the bond angle between top Ni-apical O and bottom Ni-apical O exactly 180° . The space group of HP phase is $Fmmm$ [12] or $I4/mmm$ under higher pressure [56] with 2 Ni per unit cell (1 in each layer). On the other hand, the bond angle tilts away to 168° in the LP phase. And the nearest-neighbor octahedra tilting angle alternates as the (π, π) Neel order. The space group of LP becomes $Am\bar{a}m$ with 4 Ni per unit cell (2 Ni in each layer).

In the HP phase, a superconducting dome emerges around 10 GPa, reaches its maximum T_c near 20 GPa, and gradually disappears around 90 GPa. As illustrated in Fig. 5(b), the electrical resistance $R(T)$ measured at 20.5 GPa using a diamond anvil cell (DAC) shows a clear superconducting transition beginning at 66 K (T_c), with zero resistance reached at approximately 40 K (T_c^0) [49]. A definitive signature of superconductivity is the Meissner effect, which confirms bulk superconductivity through the observation of diamagnetism. However, due to limited sample quality, measurements of the magnetic response and superconducting volume fraction in the HP phase have been subject to significant debate [57, 58].

This debate has been substantially addressed by recent experiments on $\text{La}_2\text{PrNi}_2\text{O}_7$ [13]. As shown in Fig. 5(d), the a.c. magnetic susceptibility $\chi'(T)$ was measured using the mutual induction method in a multianvil press, with a FeSe single crystal used as a calibration reference. At 9 GPa, FeSe shows a clear superconducting diamagnetic signal below 30 K. Notably, FeSe is known to transition into a non-superconducting hexagonal phase above 10 GPa, eliminating its diamagnetic response. In contrast, $\text{La}_2\text{PrNi}_2\text{O}_7$ begins to exhibit strong diamagnetic signals above 15 GPa. By comparing $\chi'(T)$ between the two samples, the superconducting shielding volume fraction in $\text{La}_2\text{PrNi}_2\text{O}_7$ was estimated to exceed 90%, providing compelling evidence for bulk superconductivity in the HP phase.

Beyond the HP superconducting phase, the LP phase of $\text{La}_3\text{Ni}_2\text{O}_7$ also exhibits intriguing behavior. The LP phase undergoes a density wave transition around 110 K and 153 K from resistance kinks [49, 59]. This transition appears to be weak and is nearly undetectable in heat capacity measurements [59]. With increasing pressure, the temperature of this resistance kink systematically decreases. In parallel, various spectroscopic and scattering techniques, including nuclear magnetic resonance (NMR), resonant inelastic X-ray scattering (RIXS), muon spin relaxation (μSR), and neutron diffraction, have reported signatures consistent with the onset of a spin density wave (SDW) state near 150 K [60–63]. However, the precise magnetic structure of $\text{La}_3\text{Ni}_2\text{O}_7$ remains under debate. Interestingly, the SDW transition temperature (T_{SDW}) increases with applied pressure, while the resistance kink decreases, suggesting the presence of two distinct density wave transitions. It is widely hypothesized that, in addition to the SDW, a charge density wave (CDW) transition also occurs. Clarifying the interplay between these two density wave orders is essential for understanding the complex phase diagram of $\text{La}_3\text{Ni}_2\text{O}_7$.

The transition from the LP to HP crystal structure in $\text{La}_3\text{Ni}_2\text{O}_7$ has been identified by synchrotron X-ray diffraction to occur between 9 and 11 GPa [12, 13], and is likely of first-order nature. Notably, the pressure required to induce superconductivity in this system is relatively modest, especially when compared to extremely high-pressure superconductors such as H_3S . In fact, superconductivity in polycrystalline $\text{La}_3\text{Ni}_2\text{O}_7$ samples has been observed at pressures as low as 6 GPa [64]. These observations suggest that conventional electron-phonon coupling is unlikely to be the primary mechanism behind the high superconducting transition temperature. Instead, the key factor appears to be the stabilization of the HP crystal structure itself. This idea is further supported by recent progress in $\text{La}_3\text{Ni}_2\text{O}_7$ thin films, where similar structural stabilization strategies have been employed to approach the superconducting phase [65].

B. Electronic structure and apical oxygen vacancy

In this subsection, we discuss the electronic structure of $\text{La}_3\text{Ni}_2\text{O}_7$ in its HP structure. The LP phase can be understood from band folding owing to its unit cell doubling. In

analogy to the single CuO_2 plane in cuprates, the electronic structure of the bilayer NiO_2 plane plays the key role. From the quantum chemistry perspective, two $\text{Ni}^{2.5+}$ atoms, under an octahedral crystal field, have fully filled t_{2g} orbitals, and additional 3 electrons filling the e_g orbitals, as illustrated in Fig. 5(c). The apical oxygen mediated interlayer hopping significantly split the $d_{3z^2-r^2}$ orbital into bonding ($d_{3z^2-r^2}^+$) and antibonding ($d_{3z^2-r^2}^-$) orbitals. $d_{x^2-y^2}$ interlayer hopping is relatively weaker. On the other hand, the Jahn–Teller distortion also contributes to raising the energy of the $d_{x^2-y^2}$ orbital relative to the $d_{3z^2-r^2}$ orbital. Hence, it tends to fully occupy the $d_{3z^2-r^2}^+$ band and quarter fill the two $d_{x^2-y^2}$ orbitals based on the atomic energy levels.

From the band structure perspective and density functional theory (DFT) calculation, the low-energy physics is formed by the bilayer e_g orbitals. Therefore, one can use the bilayer $d_{x^2-y^2}$ and $d_{3z^2-r^2}$ to construct a two-orbital bilayer tight-binding (TB) model [66]. Their band structure and orbital contents are plotted in Fig. 6(a). Generally speaking, there are four sets of bands, which are normally named as α , β , γ and δ . However, we want to remind readers that DFT calculations in strongly correlated systems highly depend on the way treating correlation and exchange-correlation functionals [67, 68]. Although the topography of the band structure is similar, the Fermi surface (FS) features vary on the different methods as illustrated in Fig. 6(b). For example, the γ band becomes fully occupied using hybrid functionals instead of a hole pocket using generalized gradient approximation (GGA) functionals [67, 68]. The only way to justify these calculations is the experimental findings. Especially, FS is always the key information for any superconductivity. It is originally thought that the high density of states γ pocket is the key factor for realizing superconductivity in $\text{La}_3\text{Ni}_2\text{O}_7$ [12]. But decisive experiments under high pressure are needed to support this conjecture originated from DFT calculations.

From the symmetry point of view, the four bands can be further split into two sectors: inversion symmetric (α and γ) and inversion antisymmetric (β and δ). One can do irreducible representation analyses for each sector. For the inversion symmetric case in Fig. 6(c), we can find that the α band and γ are well separated. Therefore, each band in the inversion symmetric sector can be Wannierized separately. The Wannierization is more complicated in inversion antisymmetric sector [68]. As plotted in Fig. 6(d), although the A_{1u} band is slightly above the B_{1u} band at Γ , they switch positions at M point. Hence, the inversion antisymmetric bands are highly entangled and one cannot write down an isolated Wannier function for each band separately. This feature indicates that although β -FS mostly contains $d_{x^2-y^2}$, the $d_{3z^2-r^2}$ component can not be ignored from a Wannierization perspective [68].

From the above discussion, we can find that the apical oxygen plays an important role in the electronic structure of $\text{La}_3\text{Ni}_2\text{O}_7$. Especially, the coupling between two Ni layers is through this apical oxygen. Defects, especially oxygen vacancies, are unavoidable factors in oxide sample growth. Experimentally, the scanning transmission electron microscopy (STEM) has been applied to study defect structures in $\text{La}_3\text{Ni}_2\text{O}_{7-\delta}$ [69]. STEM can directly image the elec-

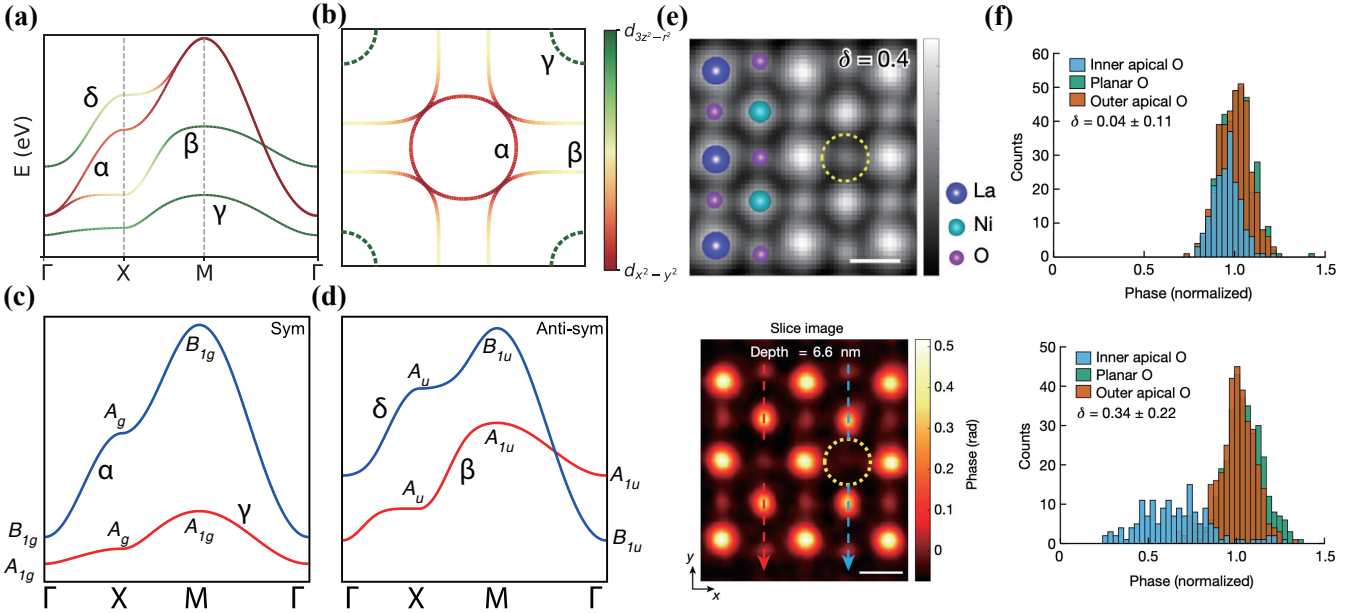


FIG. 6. (a) The HP band structure of $\text{La}_3\text{Ni}_2\text{O}_7$ and its projections into e_g orbitals. (b) Fermi surfaces of $\text{La}_3\text{Ni}_2\text{O}_7$, featuring two prominent sheets: the β -FS and the α -FS. The presence of a γ -FS at the BZ corner crossing the Fermi level remains under debate [67, 68]. (c) The four low-energy bands of $\text{La}_3\text{Ni}_2\text{O}_7$ can be categorized into symmetric (Sym) and antisymmetric (Anti-Sym) sectors. Their irreducible representations have been systematically analyzed [68]. Note that the two bands in the Anti-Sym sector are strongly entangled. (d) Simulated and experimentally observed STEM structures of $\text{La}_3\text{Ni}_2\text{O}_7$ [69]. Yellow circles indicate inner apical oxygen vacancies. (e) Phase histograms corresponding to different oxygen sites in regions with $\delta = 0.04$ and $\delta = 0.34$, normalized to the average phase of the outer apical oxygen sites [69]. A significant loss of inner apical oxygens is observed in the $\delta = 0.34$ region.

trostatic potential of atoms through the phase information. As plotted in Fig. 6(e), phase image of a slice can probe the absence of inner apical oxygens with the yellow dashed circles. From the statistics of oxygen contents at different positions in Fig. 6(f), the inner apical oxygens become much less in $\delta = 0.34$ region than the $\delta = 0$ region from the same $\text{La}_3\text{Ni}_2\text{O}_{7-\delta}$ sample. Hence, the inner apical oxygen vacancies are major defects and the $\text{La}_3\text{Ni}_2\text{O}_{7-\delta}$ sample shows a large inhomogeneity. Theoretically, there have already few attempts to address this problem. We hope for more findings to clarify this vacancy influence.

C. Density waves in 327

Although experimental measurements on the 327 phase under high pressure remain challenging, conventional material characterization techniques can be extensively applied to the LP phase. Methods such as NMR, RIXS, and ARPES have been instrumental in probing the physical properties of the 327 system.

Initial ^{139}La NMR measurements on polycrystalline $\text{La}_3\text{Ni}_2\text{O}_7$ samples suggested a possible density-wave-like transition below 150 K [71–73]. However, whether this transition corresponds to a SDW or a CDW remained unclear. Recent studies employing μSR , NMR, RIXS measurements, and neutron scattering, have identified an SDW transition in $\text{La}_3\text{Ni}_2\text{O}_7$ with a transition temperature T_{SDW} around 150 K. Zero-field μSR experiments on polycrystalline samples have

confirmed magnetic order below 154 K [60]. Furthermore, RIXS measurements revealed strongly dispersive magnetic excitations, which exhibit softening towards zero energy at the wavevector $(0.25, 0.25)$ [61], as shown in Fig. 7(a). This soft-mode behavior is a hallmark of translation symmetry breaking and is consistent with an SDW order along the (π, π) direction. In parallel, the temperature-dependent ^{139}La NMR spectra and nuclear spin-lattice relaxation rate ($1/T_1$) in single crystal provide clear evidence for SDW ordering below around 150 K [62], as shown in Fig. 7(b). Intriguingly, when pressure is applied, both NMR and μSR measurements show that T_{SDW} increases, a trend opposite to that observed in transport measurements where pressure suppresses this phase [62, 74]. This apparent discrepancy implies that the transition observed in transport may originate from a different kind of density-wave order, distinct from the SDW state. In addition to the SDW, the existence of a CDW order has been proposed. Recent optical conductivity measurements revealed opening of an energy gap below 115 K in single crystal [75], which may suggest the formation of a CDW order.

Although the SDW transition around 150 K has been confirmed, its exact magnetic structure is not yet fully determined and under debate. Nevertheless, a consensus from various experimental evidence points towards a “stripe-like” magnetic order. Specifically, RIXS studies have proposed two possibilities: a spin-charge stripe order or a double spin-stripe order. μSR data from polycrystalline samples are qualitatively consistent with the spin-charge stripe scenario [60]. In single crystal, the anisotropic splitting in the ^{139}La NMR spectra

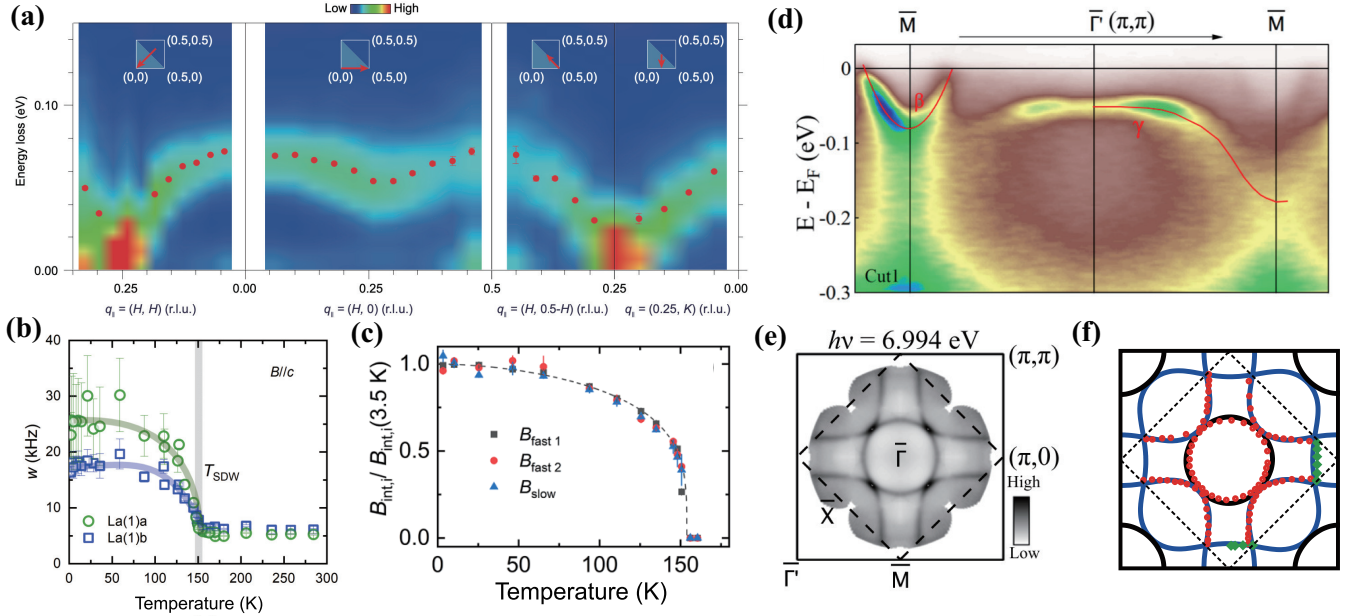


FIG. 7. (a) RIXS intensity maps along high-symmetry directions in low-pressure (LP) $\text{La}_3\text{Ni}_2\text{O}_7$, with red-filled circles marking the peak positions of magnetic excitations. Notably, the magnetic excitation spectrum becomes gapless at $Q = (\pi/2, \pi/2)$ [61]. (b) Temperature-dependent NMR linewidths for the La(1)a and La(1)b sites, indicating a SDW transition at 150 K in LP $\text{La}_3\text{Ni}_2\text{O}_7$ [62]. (c) Temperature evolution of the magnetic order parameter measured via μSR , confirming magnetic ordering in the LP phase [60]. (d) ARPES measurements of the band structure in LP $\text{La}_3\text{Ni}_2\text{O}_7$ [70]. (e) Laser-based ARPES mapping of the Fermi surface in the same LP phase [70]. (f) Fermi surface calculated using hybrid functional DFT, showing excellent agreement with the experimental ARPES data in (e), as indicated by the red and green points [67].

suggests the formation of a possible double spin-stripe with magnetic moments aligned along the c -axis [62]. Interpretation of nuclear quadrupole resonance (NQR) data on polycrystalline samples remain divergent. Yashima et al. suggests a single SDW transition corresponding to a spin-charge stripe order [76], while Luo et al. reports the simultaneous occurrence of both SDW and CDW transitions near 150 K [77]. More recently, neutron scattering on polycrystalline samples indicates the existence of two distinct spin-charge stripe orders. This model features alternating large and small magnetic moments within the Ni-O layer, which are then stacked antiferromagnetically along the c -axis, characterized by two vectors: $q_1 = (\pi/2, \pi/2, 0)$ and $q_2 = (\pi/2, \pi/2, \pi)$, corresponding to coexisting two different magnetic configurations in the system [63]. A major reason for the current uncertainty surrounding the magnetic structure may lie in the inhomogeneity of currently available samples. ^{139}La NMR and NQR studies have revealed that there are two distinct chemical sites for lanthanum atoms, both for those located between the Ni-O bilayers and for those outside the bilayers [62]. This strongly implies the coexistence of two different structural phases within the systems, which introduces an additional complexity to the experimental determination of its intrinsic magnetic structure. Therefore, further investigations using more homogeneous single crystals are imperative for accurately determining the magnetic configuration.

Both synchrotron-based and laser-based ARPES have been applied to LP phase [70], as plotted in Fig. 7(d). The band

structure of LP-327 has similar components to the HP phase. But owing to the octahedra tilting, the translation symmetry is broken to $\sqrt{2} \times \sqrt{2}$ of HP. Any eigenenergy $E(k + Q)$ with $Q = (\pi, \pi)$ in the HP BZ is folded to $E(k)$ in the new smaller BZ. Crossing points of the original bands and folded bands open gaps. From Fig. 7(d), we can see the γ band lies below the Fermi level with band top around -50 meV. Both β and α bands are observed with renormalization. For FS, the β FS center around M is folded to centering around the Γ point, resulting in a topography in Fig. 7(e). The FS feature and electronic structure in HP can be well captured by a hybrid functional DFT calculation and its further correlation method Fig. 7(f) [67].

D. 327 thin film

Following the discovery of high- T_c SC in $\text{La}_3\text{Ni}_2\text{O}_7$ under high pressure, numerous efforts have been made to synthesize superconducting thin films at ambient pressure. As previously discussed, stabilizing the $\text{La}_3\text{Ni}_2\text{O}_7$ structure is essential for the emergence of superconductivity. It is well established that compressive or tensile strain effectively mimics the key electronic structure modifications induced by high pressure [78]. As such, strain offers an alternative pathway to stabilize the high-pressure phase of the 327 compound, as illustrated in Fig. 8(a). After extensive work using SrLaAlO_4 (SLAO) substrates, several groups have successfully reported supercon-

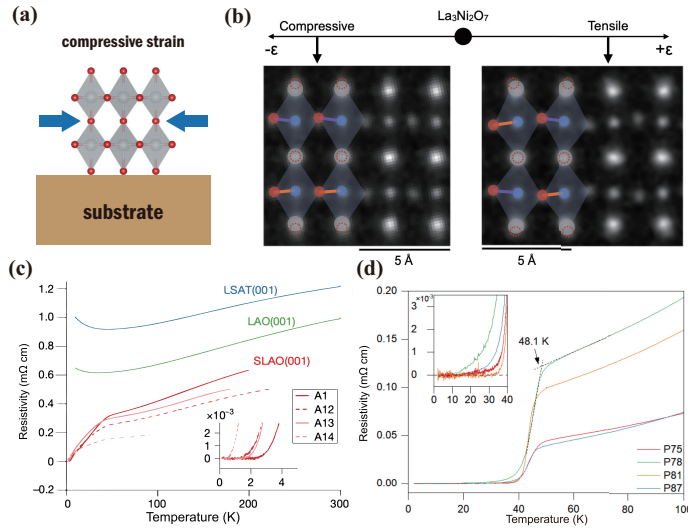


FIG. 8. (a) Schematic illustration of the compressive strain induced by the substrate during thin-film deposition. (b) STEM images of $\text{La}_3\text{Ni}_2\text{O}_7$ thin films grown under compressive and tensile strain conditions [83]. (c) Temperature-dependent resistivity of $\text{La}_3\text{Ni}_2\text{O}_7$ thin films on various substrates [65]. Films grown on compressive SLAO substrates exhibit a broad superconducting transition. A1, A12, A13, and A14 denote different sample identifiers. (d) Resistivity measurements of $\text{La}_2\text{PrNi}_2\text{O}_7$ thin films, showing a superconducting transition onset above 48.1 K. Sample labels include P75, P78, P81, and P87 [80].

ducting 327-based films: Eun-Kyo Ko et al. reported superconducting 327 films [65]; Guangdi Zhou et al. demonstrated superconductivity in $\text{La}_{2.85}\text{Pr}_{0.15}\text{Ni}_2\text{O}_7$ [79]; Yidi Liu et al. reported superconducting $\text{La}_2\text{PrNi}_2\text{O}_7$ films [80]; Bo Hao et al. observed superconductivity in $\text{La}_{3-x}\text{Sr}_x\text{Ni}_2\text{O}_7$ films [81]; and Baiyang Wang et al. successfully grew $\text{La}_2\text{PrNi}_2\text{O}_7$ films using the oxide MBE method [82], a resistivity drop was also observed in the transport measurements.

The temperature-dependent resistivity $\rho(T)$ of $\text{La}_3\text{Ni}_2\text{O}_7$ thin films grown on different substrates is shown in Fig. 8(c). On SLAO substrates, $\rho(T)$ exhibits a drop below 42 K, reaching zero resistance at approximately 2 K (T_c^0). In contrast, films grown on LaAlO_3 (LAO) and $(\text{LaAlO}_3)_{0.3}(\text{Sr}_2\text{TaAlO}_6)_{0.7}$ (LSAT) show a resistivity upturn below roughly 40 K, without a zero-resistance transition. Structurally, the strain imposed on the film by the substrate can be quantified as $\epsilon = \frac{a_s - a_f}{a_f}$, where a_s and a_f are the in-plane lattice constants of the substrate and the film without substrate constraints, respectively. The bulk in-plane lattice parameters can be used as an approximation for a_f . The in-plane pseudotetragonal lattice constants (a and b axes) of bulk 327 are approximately 3.83 Å. SLAO, with $a_s = 3.75$ Å, introduces about -2% in-plane compressive strain [83]. Multislice electron ptychography has been used to study the atomic-scale structural evolution of 327 films under varying strain conditions induced by different substrates, as shown in Fig. 8(b) [83]. These results demonstrate that compressive strain ($\epsilon < 0$) favors the stabilization of the HP phase, while tensile strain ($\epsilon > 0$) tends to preserve the LP structure, as

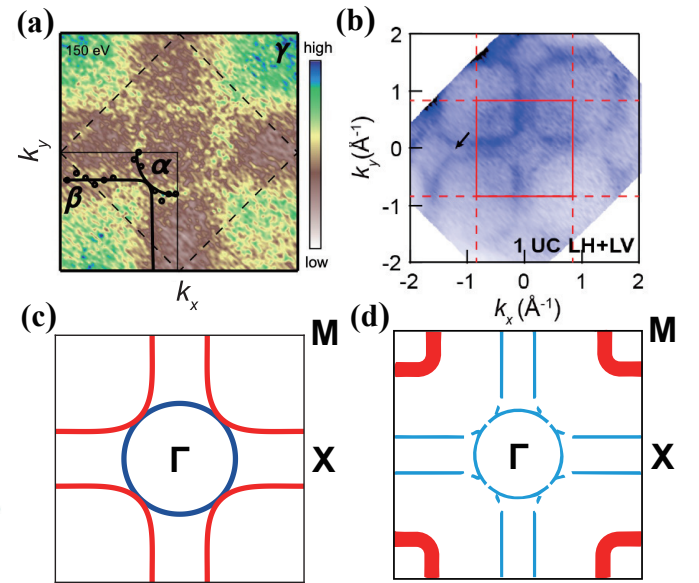


FIG. 9. (a, c) ARPES-measured and schematic Fermi surfaces of $\text{La}_2\text{PrNi}_2\text{O}_7$ [82], showing that the γ band does not cross the Fermi level. (b, d) ARPES-measured and schematic Fermi surfaces of $\text{La}_{2.85}\text{Pr}_{0.15}\text{Ni}_2\text{O}_7$ [84], where the γ band crosses the Fermi level.

expected.

Compared to the bulk structure under pressure, the c -axis of the 327 thin film expands to 20.6 Å [83]. Our DFT calculations reveal that the Jahn-Teller distortion is more sensitive to structural changes than interlayer coupling. As shown in Fig. 5(c), the Jahn-Teller distortion, like interlayer coupling, lowers the energy of the bonding $d_{3z^2-r^2}^+$ orbital. Therefore, both effects should be treated on equal footing.

Another critical factor in realizing superconductivity in 327 thin films is ozone annealing. It has been widely reported that many as-grown 327 films are insulating prior to annealing, indicating that disorder, inhomogeneity, and structural defects are unavoidable considerations in the superconducting behavior of these films. In particular, apical oxygen vacancies are believed to play an important role in shaping the electronic properties. Recent studies suggest that planar oxygen vacancies become predominant in superconducting 327 samples [81].

The development of superconducting 327 films has progressed rapidly. Notably, substantial improvements have been achieved in $\text{La}_2\text{PrNi}_2\text{O}_7$ films [80]. As shown in Fig. 8(d), the maximum onset temperature T_c reaches 48.1 K, with zero resistance achieved at temperatures exceeding 30 K. Interestingly, the normal-state transport in $\text{La}_2\text{PrNi}_2\text{O}_7$ exhibits clear Fermi-liquid behavior, and its Hall resistivity closely resembles that of overdoped $\text{La}_{1.75}\text{Sr}_{0.25}\text{CuO}_4$ [80, 85]. More recently, a superconducting dome has also been observed in Sr-doped $\text{La}_{3-x}\text{Sr}_x\text{Ni}_2\text{O}_7$ thin films, further establishing the tunability and richness of the 327 film phase diagram [81]. Additionally, applying high pressure to strain-engineered 327 thin films has further enhanced transition temperature, reaching a maximum T_c of approximately 60 K [86].

Several ARPES studies have been carried out to investigate

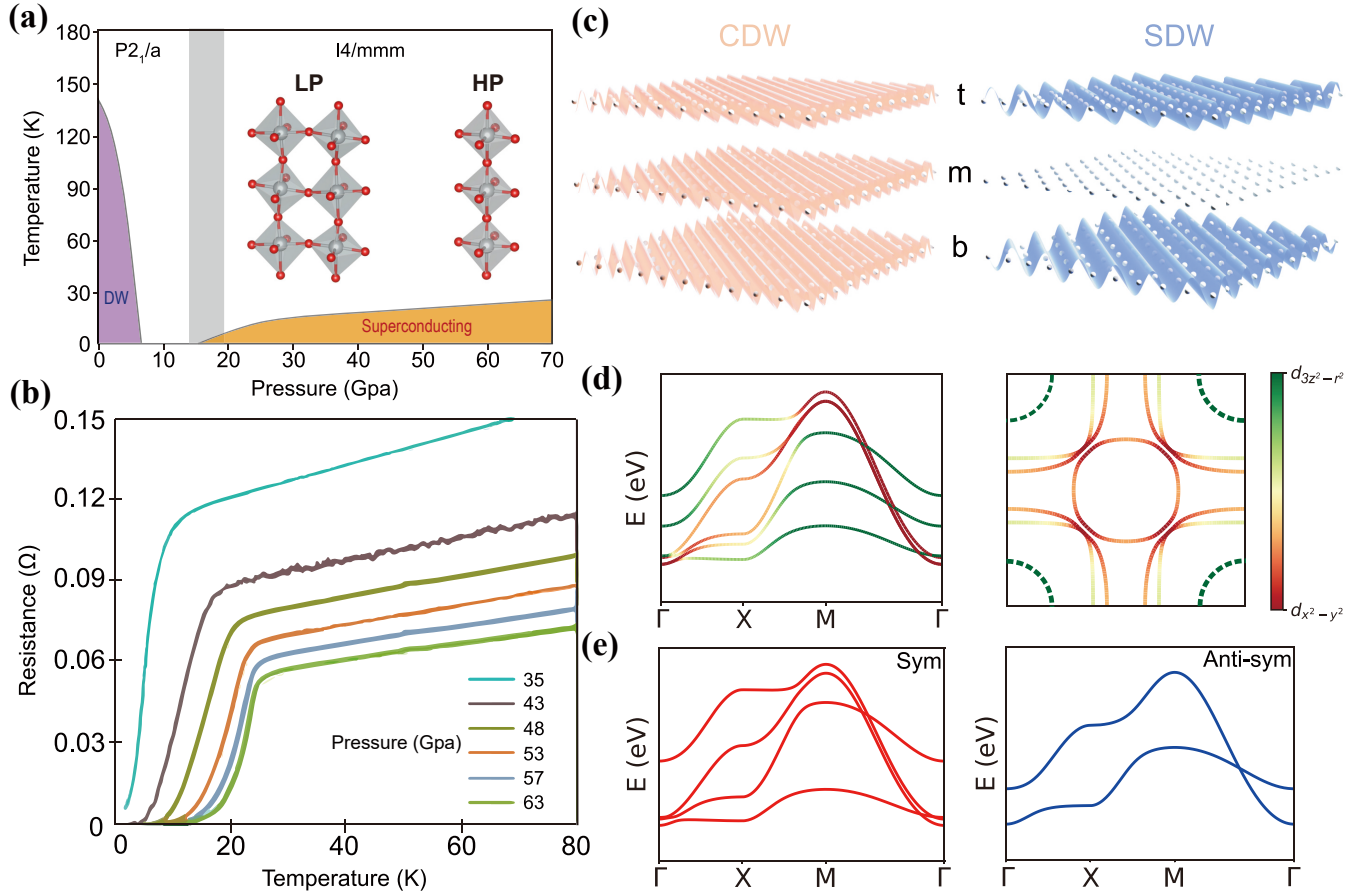


FIG. 10. (a) Phase diagram of $\text{La}_4\text{Ni}_3\text{O}_{10}$ [14], featuring both LP and HP phases. The LP phase exhibits a pronounced DW transition, while superconductivity emerges in the HP phase under pressure. (b) Resistivity of $\text{La}_4\text{Ni}_3\text{O}_{10}$ measured under varying pressures, showing a superconducting transition [14]. (c) Density wave phases in the 43(10) compound. The trilayer is commonly labeled as top (t), middle (m), and bottom (b) layers. Notably, the CDW exists in all three layers, whereas the SDW is present only in the top and bottom layers [87]. (d) Band structure and Fermi surfaces of $\text{La}_4\text{Ni}_3\text{O}_{10}$. The presence of the $d_{3z^2-r^2}$ Fermi surface pocket at the Brillouin zone corner remains unresolved. (e) The band structure can also be decomposed into symmetric and antisymmetric sectors, with the symmetric sector resembling that of $\text{La}_3\text{Ni}_2\text{O}_7$.

the key electronic features underlying superconductivity in 327 thin films [82, 84, 88]. Overall, the observed band structure in these superconducting films resembles that of the LP phase, as shown in Fig. 7(d), where the α , β , and γ bands are commonly identified. Among these, the γ band—particularly its position relative to the Fermi level—has attracted special attention, given that FS topology is a crucial factor for understanding superconductivity. As shown in Fig. 9, ARPES measurements on $\text{La}_2\text{PrNi}_2\text{O}_7$ and $\text{La}_{2.85}\text{Pr}_{0.15}\text{Ni}_2\text{O}_7$ films reveal distinct FS topologies. In $\text{La}_2\text{PrNi}_2\text{O}_7$, there is no γ pocket observed; its band top lies approximately 70 meV below the Fermi level, even deeper than the 50 meV observed in the LP phase. In contrast, the γ band in $\text{La}_{2.85}\text{Pr}_{0.15}\text{Ni}_2\text{O}_7$ crosses the Fermi level, forming a small pocket, as plotted in Fig. 9(b,d). These contrasting results likely stem from differences in sample thickness, composition, strain, interfacial reconstruction, or growth conditions. Nonetheless, the absence of a γ pocket in superconducting $\text{La}_2\text{PrNi}_2\text{O}_7$ suggests that the γ band is not essential for superconductivity in the 327 system.

E. Theory of 327

Finally, we want to briefly mention theoretical proposals for high- T_c superconductivity in 327. Generally speaking, there are two approaches for the pairing mechanism of high- T_c superconductors: weak-coupling and strong-coupling. Weak-coupling theories focus on Fermi surface instabilities and typically employ methods such as the random phase approximation [66, 89–98] or functional renormalization group [99–101]. In contrast, strong-coupling theories begin from a Mott insulating or magnetically ordered state driven by strong electron correlations, with superconductivity emerging upon doping, as described by $t - J$ or related models [102–113]. At present, it remains unclear which framework is more appropriate for 327. However, any viable theory must be grounded in experimental observations, particularly the Fermi surface revealed by recent ARPES measurements.

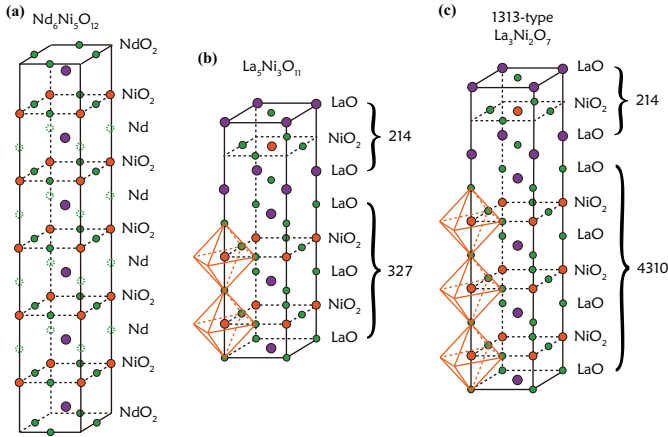


FIG. 11. (a) Crystal structure of $\text{Nd}_6\text{Ni}_5\text{O}_{10}$ [17], obtained by reducing the Ruddlesden-Popper phase $\text{Nd}_6\text{Ni}_5\text{O}_{16}$. (b) Crystal structure of $\text{La}_5\text{Ni}_3\text{O}_{11}$ [18], formed by inserting a La_2NiO_4 layer into the bilayer $\text{La}_3\text{Ni}_2\text{O}_7$ structure. This compound is also referred to as the 1212 phase. (c) Alternative crystal structure of $\text{La}_3\text{Ni}_2\text{O}_7$ [58], composed of a trilayer $\text{La}_4\text{Ni}_3\text{O}_7$ unit and a La_2NiO_4 block. This structure is known as the 1313 phase.

IV. 43(10) AND OTHER MULTILAYER NICKELATES

A. 43(10)

The trilayer 43(10) is another case of superconductors under pressure. In the thermodynamic phase diagram, the 43(10) is more stable than 327. The single crystal quality becomes much better than 327. The general phase diagram under pressure and temperature of 43(10) is plotted in Fig. 10 [14]. The phase diagram is also separated into two phases, the high-pressure $I4/mmm$ phase and the lower-pressure $P2_1/a$ phase. Similar to 327, the three NiO_6 octahedra line up in the HP structure while they tilt away 180° Ni-O-Ni bond angles in the LP structure.

The transport measurements of 43(10) under pressure in the helium DAC are plotted in Fig. 10(b). After the structural transition around 15 GPa, the HP phase of 43(10) starts to drop in resistance below a critical temperature. The zero resistances are observed above 43.0 GPa. The superconducting T_c onset can reach around 30 K. The d.c. magnetic susceptibility measurements on 43(10) further confirm the diamagnetic response above 30 GPa.

The LP phase undergoes a density wave transition around 136 K at ambient pressure. This density wave transition becomes much sharper than 327. The heat capacity shows an obvious transition around 136 K. The previous single crystal synchrotron x-ray and neutron diffraction have revealed intertwined density waves with a layer-dependent feature in this trilayer structure [87]. As shown in Fig. 10(c), the SDW displays a node on the inner Ni-O plane while maintaining an out-of-phase between the two outer Ni-O planes. In contrast, the CDW persists across all Ni-O layers with an in-phase [87]. In addition, the CDW and SDW exhibit incommensurate propagation vectors $\mathbf{q}_c = (0, q_c, 0)$ and $\mathbf{q}_s = (0, 1 - q_s, 0)$, respectively, with $q_c = 2q_s$ as expected for a sys-

tem with coupled charge and spin order [87]. Direct visualization of an incommensurate unidirectional CDW has also been observed by scanning tunneling microscopy (STM) [114]. Complementary experiments, including μSR [115, 116] and NMR measurements [71–73], have independently identified a density wave transition with a transition temperature $T_{\text{DW}} \approx 135$ K. Furthermore, a distinct formation of a density wave energy gap is revealed by optical conductivity, pump-probe and ARPES measurements [117–120]. Under applied pressure, transition temperatures of both CDW and SDW were suppressed [116, 121], which contrasts with the double-layer RP nickelate $\text{La}_3\text{Ni}_2\text{O}_7$ [62, 74]. Moreover, two μSR studies report an additional order of SDW at a lower temperature $T_{\text{SDW}2} \approx 80$ K in both single crystal and polycrystalline $\text{La}_4\text{Ni}_3\text{O}_{10}$ samples [115, 116]. However, the underlying mechanism, whether involving a spin reorientation, a phase separation or other phenomena, still remains unclear [115, 116].

The electronic structure of 43(10) becomes more complicated than 327. As discussed above, the RP trilayer structure comes from a bilayer 327 with an additional LaNiO_3 layer. It is better to classify its band structures into two groups, inversion symmetric and inversion antisymmetric. Using the labeling top (t), middle (m), bottom (b) of the trilayer NiO_2 planes, the symmetric bands formed by $\frac{1}{\sqrt{2}}(\psi_t + \psi_b)$ and ψ_m while the antisymmetric bands formed by $\frac{1}{\sqrt{2}}(\psi_t - \psi_b)$. As shown in Fig. 10(d), the symmetric bands contain four bands, which shows a similar contour of 327. On the other hand, the antisymmetric bands host two bands like a single-layer two-orbital model. There are also theoretical groups proposing to further split the symmetric bands. However, due to the on-site energy of the middle is always different from the top and bottom. It is not convenient to treat them separately, especially under electron correlation. With this information, one can easily understand the FS of 327. Two FSs from symmetric bands like 327, and another additional FS from the antisymmetric band.

B. Other Multilayer Nickelates

Besides 112, 327, 43(10), there are other multilayer nickelate superconductors or related structures, as plotted in Fig. 11. We briefly list these findings in this short section.

We have shown that LaNiO_2 comes from the oxygen reduction of LaNiO_3 . Therefore, it is natural to achieve other multilayer 112 structures through the reduction of other RP nickelates. Several multilayer 112 structure thin films have been grown using oxide molecular beam epitaxy [17]. The crystal structure of $\text{Nd}_6\text{Ni}_5\text{O}_{10}$ is plotted in Fig. 11(a), where oxygens from Nd plane are removed in the RP $\text{Nd}_6\text{Ni}_5\text{O}_{16}$. One benefit from this process is that hole-doping naturally occurs. Hence, no chemical doping using Sr or other ions is needed. The $d^{8.8}$ electron filling is obtained in 5-layer $\text{Nd}_6\text{Ni}_5\text{O}_{12}$ with onset T_c around 10 K. On the other hand, $\text{Nd}_4\text{Ni}_3\text{O}_8$ with $d^{8.67}$ filling becomes outside the superconducting dome.

As discussed in the introduction, the n -layer RP nickelates can be constructed by inserting LaNiO_3 layers into the

La_2NiO_4 framework. Conversely, it is also possible to incorporate La_2NiO_4 layers into RP structures. This concept is realized in the compound $\text{La}_5\text{Ni}_3\text{O}_{11}$ [18], which can be viewed as a hybrid of $\text{La}_3\text{Ni}_2\text{O}_7$ and La_2NiO_4 . In $\text{La}_5\text{Ni}_3\text{O}_{11}$ shown in Fig. 11(b), single-layer and bilayer NiO_6 octahedral blocks alternate along the c -axis, forming a unique hybrid RP nickelate known as the 1212 phase. Similar to $\text{La}_3\text{Ni}_2\text{O}_7$, $\text{La}_5\text{Ni}_3\text{O}_{11}$ exhibits a density-wave transition near 170 K. However, unlike $\text{La}_3\text{Ni}_2\text{O}_7$ and $\text{La}_4\text{Ni}_3\text{O}_{10}$, the transition temperature in $\text{La}_5\text{Ni}_3\text{O}_{11}$ increases steadily with pressure, reaching approximately 210 K at 12 GPa, before abruptly vanishing prior to the onset of pressure-induced superconductivity at higher pressures. The maximum T_c observed in $\text{La}_5\text{Ni}_3\text{O}_{11}$ is 64 K, which is slightly lower than that of $\text{La}_3\text{Ni}_2\text{O}_7$. High-pressure synchrotron X-ray diffraction reveals a structural phase transition in $\text{La}_5\text{Ni}_3\text{O}_{11}$ from an orthorhombic to a tetragonal symmetry at around 4.5 GPa. Interestingly, unlike in $\text{La}_3\text{Ni}_2\text{O}_7$ and $\text{La}_4\text{Ni}_3\text{O}_{10}$, this structural transition does not significantly affect either the density-wave state or the superconducting properties in $\text{La}_5\text{Ni}_3\text{O}_{11}$.

In addition to $\text{La}_3\text{Ni}_2\text{O}_7$, recent studies have reported the coexistence of an alternating monolayer–trilayer phase, known as the 1313 phase, alongside the bilayer $\text{La}_3\text{Ni}_2\text{O}_7$ structure [58, 122]. The crystal structure of the 1313 phase is illustrated in Fig. 11(c). Previous high-pressure transport measurements indicate the potential for high-temperature superconductivity in the 1313 phase, with an onset transition temperature of around 80 K. However, considering that the T_c of the trilayer compound $\text{La}_4\text{Ni}_3\text{O}_{10}$ is only around 30 K, it is likely that the observed superconductivity in the 1313 phase originates from residual bilayer $\text{La}_3\text{Ni}_2\text{O}_7$, which is inevitably present in the 1313. The intrinsic physical properties of the 1313 phase, as well as its influence on the superconducting behavior of the 327 system, remain open questions and warrant further detailed experimental and theoretical investigation.

V. PERSPECTIVE

The discovery of superconductivity in nickelates has revitalized interest in the broader field of unconventional superconductors. In this article, we have reviewed the recent significant advances in the study of nickelate superconductors. However, critical challenges and opportunities remain across several key aspects that are shaping the future direction of nickelate research.

- *Sample quality:* The synthesis of high-quality nickelate samples—both thin films and single crystals—remains a critical bottleneck in the field. Achieving high-quality samples is essential for definitive conclusions. Especially, the 327 sample quality still requires significant

improvement.

- *Electronic structure:* Understanding the electronic structure is a fundamental step toward uncovering the origin of superconductivity and related physical phenomena. Recent ARPES studies on 112 have shed light on the interplay between 3d and rare-earth 5d electrons. More ARPES findings on superconducting 327 hold promise for deepening our understanding of the electronic nature that supports superconductivity.
- *Disorder:* Disorder is an unavoidable aspect of nickelate superconductors, with apical oxygen vacancies playing a particularly critical role. Elucidating the impact of such disorder requires further theoretical and experimental investigation.
- *Innovative material characterization:* Current material characterization techniques are largely constrained to thin-film samples and high-pressure environments. To advance the field, the development of more innovative and versatile characterization methods is essential.
- *Pairing symmetry:* Identifying the pairing symmetry is a crucial step in understanding unconventional superconductors. However, definitive conclusions remain elusive, largely due to limitations in sample quality and the challenges associated with current characterization techniques.
- *Difference between cuprates and nickelates:* Insights from the study of nickelates may provide valuable clues for resolving the enduring mysteries surrounding cuprate superconductors. Table I presents a comparison between these two families. By highlighting both their similarities and differences, we hope this comparison will contribute to the development of a unified framework for understanding high-temperature superconductivity.
- *Implication for discovering new high- T_c superconductors:* The newly discovered nickelate superconductors may also establish important guidelines for searching for new high- T_c materials. As shown in Table I, there exist two distinct electronic environments that can host high- T_c superconductivity. These environments are consistent with the recently proposed “genes” framework for unconventional high- T_c superconductors [123, 124], in which the transition metal d -orbitals strongly hybridized with the oxygen p -orbitals are isolated near the Fermi energy. With the discovery of new high- T_c superconductors, summarizing their common features to guide the search for other novel high- T_c materials is also a worthwhile direction of exploration.

VI. ACKNOWLEDGE

We thank Fu-Chun Zhang, Tao Xiang, Donglai Feng, Meng Wang, Guangming Zhang, Qianghua Wang, Yijun Yu, Dan-

feng Li, Huiqiu Yuan, Xingjiang Zhou, Zhen Chen, Ke-Jin

	Cuprates	LaNiO ₂	La ₃ Ni ₂ O ₇	La ₄ Ni ₃ O ₁₀
Layered Structures	2D CuO ₂ planes	2D NiO ₂ planes	Bilayer NiO ₂ planes	Trilayer NiO ₂ planes
Valence State	Cu ²⁺ (3d ⁹)	Ni ¹⁺ (3d ⁹)	Ni ^{2.5+} (3d ^{7.5})	Ni ^{2.67+} (3d ^{7.33})
Orbital Character	3d _{x²-y²}	3d _{x²-y²} hybridized with rare-earth orbitals	3d _{x²-y²} , 3d _{3z²-r²}	3d _{x²-y²} , 3d _{3z²-r²}
Parent State	Charge Transfer insulator	Mott insulator (without rare-earth)	Open question	Open question
Superconductivity	<i>d</i> -wave SC	Evidence of <i>d</i> -wave SC	pressure or thin film, symmetry unknown	pressure, symmetry unknown
T _c	~135 K	~15–40 K	~80 K (high pressure) 48 K (thin film)	~40 K (high pressure)
Correlation Strength	Strong	Strong	Strong or intermediate	Strong or intermediate
Electron-Phonon for SC	×	Unlikely	Unlikely	Unlikely

TABLE I. Comparison between Cuprate, LaNiO₂, La₃Ni₂O₇, and La₄Ni₃O₁₀ superconductors.

Zhou, Dawei Shen, Junfeng He, Yuefeng Nie, Lei Shu, Jun Zhao, Ariando Ariando, Bai Yang Wang, Kyle Shen, Berit Goodge et. al. for useful discussions.

K.J. and J.P.H. acknowledge the support of the National Natural Science Foundation of China (Grant NSFC-12494594, No. NSFC-12174428), the New Cornerstone Investigator Program. K.J., J.J.Y., and W.T. acknowledge the Chinese Academy of Sciences Project for Young Scientists in Basic Research (2022YSBR-048). J.J.Y. acknowledges sup-

port from the National Natural Science Foundation of China (Grant NSFC-12494592). W.T. acknowledges the National Natural Science Foundation of China (Grant No. 12325403). W.T. and X.H.C. acknowledge the National Key R&D Program of the MOST of China (Grant 2022YFA1602601). W.T., J.J.Y., and X.H.C. acknowledge the Chinese Academy of Sciences under contract No. JZHKYPT-2021-08. J.G.C. acknowledges support from the National Natural Science Foundation of China (Grant NSFC-12025408, U23A6003), and the National Key R&D Program of China (2023YFA1406100).

[1] J. G. Bednorz and K. A. Müller, “Possible high-*tc* superconductivity in the Ba-La-Cu-O system,” *Zeitschrift für Physik B Condensed Matter* **64**, 189–193 (1986).

[2] Patrick A. Lee, Naoto Nagaosa, and Xiao-Gang Wen, “Doping a mott insulator: Physics of high-temperature superconductivity,” *Rev. Mod. Phys.* **78**, 17–85 (2006).

[3] B. Keimer, S. A. Kivelson, M. R. Norman, S. Uchida, and J. Zaanen, “From quantum matter to high-temperature superconductivity in copper oxides,” *Nature* **518**, 179–186 (2015).

[4] Yoichi Kamihara, Takumi Watanabe, Masahiro Hirano, and Hideo Hosono, “Iron-Based Layered Superconductor La[O_{1-x}F_x]FeAs (x=0.05–0.12) with T_c =26K,” *Journal of the American Chemical Society* **130**, 3296–3297 (2008).

[5] Hiroki Takahashi, Kazumi Igawa, Kazunobu Arii, Yoichi Kamihara, Masahiro Hirano, and Hideo Hosono, “Superconductivity at 43 K in an iron-based layered compound LaO_{1-x}F_xFeAs,” *Nature* **453**, 376–378 (2008).

[6] Johnpierre Paglione and Richard L. Greene, “High-temperature superconductivity in iron-based materials,” *Nature Physics* **6**, 645–658 (2010).

[7] V. I. Anisimov, D. Bakhvalov, and T. M. Rice, “Electronic structure of possible nickelate analogs to the cuprates,” *Phys. Rev. B* **59**, 7901–7906 (1999).

[8] K.-W. Lee and W. E. Pickett, “Infinite-layer LaNiO₂: Ni¹⁺ is not Cu²⁺,” *Phys. Rev. B* **70**, 165109 (2004).

[9] Danfeng Li, Kyuho Lee, Bai Yang Wang, Motoki Osada, Samuel Crossley, Hye Ryoung Lee, Yi Cui, Yasuyuki Hikita, and Harold Y. Hwang, “Superconductivity in an infinite-layer nickelate,” *Nature* **572**, 624–627 (2019).

[10] Michael R Norman, “Entering the nickel age of superconductivity,” *Physics* **13**, 85 (2020).

[11] Warren E. Pickett, “The dawn of the nickel age of superconductivity,” *Nature Reviews Physics* **3**, 7–8 (2021).

[12] Hualei Sun, Mengwu Huo, Xunwu Hu, Jingyuan Li, Zengjia Liu, Yifeng Han, Lingyun Tang, Zhongquan Mao, Pengtao Yang, Bosen Wang, Jinguang Cheng, Dao-Xin Yao, Guang-Ming Zhang, and Meng Wang, “Signatures of superconductivity near 80 K in a nickelate under high pressure,” *Nature* **621**, 493–498 (2023).

[13] Ningning Wang, Gang Wang, Xiaoling Shen, Jun Hou, Jun Luo, Xiaoping Ma, Huaixin Yang, Lifen Shi, Jie Dou, Jie Feng, Jie Yang, Yunqing Shi, Zhian Ren, Hanming Ma, Pengtao Yang, Ziyi Liu, Yue Liu, Hua Zhang, Xiaoli Dong, Yuxin Wang, Kun Jiang, Jiangping Hu, Shoko Nagasaki, Kentaro Kitagawa, Stuart Calder, Jiaqiang Yan, Jianping Sun, Bosen Wang, Rui Zhou, Yoshiya Uwatoko, and Jinguang Cheng, “Bulk high-temperature superconductivity in pressurized tetragonal La₂PrNi₂O₇,” *Nature* **634**, 579–584 (2024).

[14] Yinghao Zhu, Di Peng, Enkang Zhang, Bingying Pan, Xu Chen, Lixing Chen, Huifen Ren, Feiyang Liu, Yiqing Hao, Nana Li, Zhenfang Xing, Fujun Lan, Jiyuan Han, Junjie Wang, Donghan Jia, Hongliang Wo, Yiqing Gu, Yimeng Gu, Li Ji, Wenbin Wang, Huiyang Gou, Yao Shen, Tianping Ying, Xiaolong Chen, Wenge Yang, Huibo Cao, Changlin Zheng, Qiaoshi Zeng, Jian-gang Guo, and Jun Zhao, “Superconductivity in pressurized trilayer La₄Ni₃O_{10-δ} single crystals,” *Nature* **631**, 531–536 (2024).

[15] Mingxin Zhang, Cuiying Pei, Di Peng, Xian Du, Weixiong Hu, Yantao Cao, Qi Wang, Juefei Wu, Yidian Li, Huanyu Liu, Chenhaoping Wen, Jing Song, Yi Zhao, Changhua Li, Weizheng Cao, Shihao Zhu, Qing Zhang, Na Yu, Peihong Cheng, Lili Zhang, Zhiwei Li, Jinkui Zhao, Yulin Chen,

Changqing Jin, Hanjie Guo, Congjun Wu, Fan Yang, Qiaoshi Zeng, Shichao Yan, Lexian Yang, and Yanpeng Qi, "Superconductivity in trilayer nickelate $\text{La}_4\text{Ni}_3\text{O}_{10}$ under pressure," *Phys. Rev. X* **15**, 021005 (2025).

[16] Qing Li, Ying-Jie Zhang, Zhe-Ning Xiang, Yuhang Zhang, Xiyu Zhu, and Hai-Hu Wen, "Signature of superconductivity in pressurized $\text{La}_4\text{Ni}_3\text{O}_{10}$," *Chin. Phys. Lett.* **41**, 017401 (2024).

[17] Grace A. Pan, Dan Ferenc Segedin, Harrison LaBollita, Qi Song, Emilian M. Nica, Berit H. Goodge, Andrew T. Pierce, Spencer Doyle, Steve Novakov, Denisse Córdova Carrizales, Alpha T. N'Diaye, Padraic Shafer, Hanjong Paik, John T. Heron, Jarad A. Mason, Amir Yacoby, Lena F. Kourkoutis, Onur Erten, Charles M. Brooks, Antia S. Botana, and Julia A. Mundy, "Superconductivity in a quintuple-layer square-planar nickelate," *Nature Materials* **21**, 160–164 (2022).

[18] Mengzhu Shi, Di Peng, Kaibao Fan, Zhenfang Xing, Shaohua Yang, Yuzhu Wang, Houpu Li, Rongqi Wu, Mei Du, Binghui Ge, Zhidan Zeng, Qiaoshi Zeng, Jianjun Ying, Tao Wu, and Xianhui Chen, "Superconductivity of the hybrid Ruddlesden-Popper $\text{La}_5\text{Ni}_3\text{O}_{11}$ single crystals under high pressure," *arXiv preprint arXiv:2502.01018* (2025).

[19] F. C. Zhang and T. M. Rice, "Effective Hamiltonian for the superconducting Cu oxides," *Phys. Rev. B* **37**, 3759–3761 (1988).

[20] J. van Elp, H. Eskes, P. Kuiper, and G. A. Sawatzky, "Electronic structure of Li-doped NiO ," *Phys. Rev. B* **45**, 1612–1622 (1992).

[21] S. N. Ruddlesden and P. Popper, "The compound $\text{Sr}_3\text{Ti}_2\text{O}_7$ and its structure," *Acta Crystallographica* **11**, 54–55 (1958).

[22] A. Wold, R. J. Arnott, and J. B. Goodenough, "Some magnetic and crystallographic properties of the system $\text{LaMn}_{1-x}\text{Ni}_x\text{O}_{3+\lambda}$," *Journal of Applied Physics* **29**, 387–389 (1958).

[23] Aaron Wold and Ronald J. Arnott, "Preparation and crystallographic properties of the systems $\text{LaMn}_{1-x}\text{Mn}_x\text{O}_{3+\lambda}$ and $\text{LaMn}_{1-x}\text{Ni}_x\text{O}_{3+\lambda}$," *Journal of Physics and Chemistry of Solids* **9**, 176–180 (1959).

[24] J. Drennan, C.P. Tavares, and B.C.H. Steele, "An electron microscope investigation of phases in the system La-Ni-O," *Materials Research Bulletin* **17**, 621–626 (1982).

[25] R.A. Mohan Ram, L. Ganapathi, P. Ganguly, and C.N.R. Rao, "Evolution of three-dimensional character across the $\text{La}_{n+1}\text{Ni}_n\text{O}_{3n+1}$ homologous series with increase in n ," *Journal of Solid State Chemistry* **63**, 139–147 (1986).

[26] K. Sreedhar, M. McElfresh, D. Perry, D. Kim, P. Metcalf, and J.M. Honig, "Low-temperature electronic properties of the $\text{La}_{n+1}\text{Ni}_n\text{O}_{3n+1}$ ($n = 2, 3$, and ∞) system: Evidence for a crossover from fluctuating-valence to fermi-liquid-like behavior," *Journal of Solid State Chemistry* **110**, 208–215 (1994).

[27] Z. Zhang, M. Greenblatt, and J.B. Goodenough, "Synthesis, structure, and properties of the layered perovskite $\text{La}_3\text{Ni}_2\text{O}_{7-\delta}$," *Journal of Solid State Chemistry* **108**, 402–409 (1994).

[28] Satoshi Taniguchi, Takashi Nishikawa, Yukio Yasui, Yoshiaki Kobayashi, Jun Takeda, Shin-ichi Shamoto, and Masatoshi Sato, "Transport, magnetic and thermal properties of $\text{La}_3\text{Ni}_2\text{O}_{7-\delta}$," *Journal of the Physical Society of Japan* **64**, 1644–1650 (1995).

[29] Z. Zhang and M. Greenblatt, "Synthesis, structure, and properties of $\text{Ln}_4\text{Ni}_3\text{O}_{10-\delta}$ ($\text{Ln} = \text{La, Pr, and Nd}$)," *Journal of Solid State Chemistry* **117**, 236–246 (1995).

[30] Bai Yang Wang, Kyuho Lee, and Berit H. Goodge, "Experimental progress in superconducting nickelates," *Annual Review of Condensed Matter Physics* **15**, 305–324 (2024).

[31] Yusuke Nomura and Ryotaro Arita, "Superconductivity in infinite-layer nickelates," *Reports on Progress in Physics* **85**, 052501 (2022).

[32] M. A. Hayward, M. A. Green, M. J. Rosseinsky, and J. Sloan, "Sodium hydride as a powerful reducing agent for topotactic oxide deintercalation: Synthesis and characterization of the nickel(i) oxide LaNiO_2 ," *Journal of the American Chemical Society* **121**, 8843–8854 (1999).

[33] M.A. Hayward and M.J. Rosseinsky, "Synthesis of the infinite layer Ni(I) phase NdNiO_{2+x} by low temperature reduction of NdNiO_3 with sodium hydride," *Solid State Sciences* **5**, 839–850 (2003), international Conference on Inorganic Materials 2002.

[34] Masanori Kawai, Satoru Inoue, Masaichiro Mizumaki, Naomi Kawamura, Noriya Ichikawa, and Yuichi Shimakawa, "Reversible changes of epitaxial thin films from perovskite LaNiO_3 to infinite-layer structure LaNiO_2 ," *Applied Physics Letters* **94**, 082102 (2009).

[35] D. Kaneko, K. Yamagishi, A. Tsukada, T. Manabe, and M. Naito, "Synthesis of infinite-layer LaNiO_2 films by metal organic decomposition," *Physica C: Superconductivity* **469**, 936–939 (2009).

[36] S. Lin Er Chow, Zhaoyang Luo, and A. Ariando, "Bulk superconductivity near 40 K in hole-doped SmNiO_2 at ambient pressure," *Nature* **642**, 58–63 (2025).

[37] Mingwei Yang, Heng Wang, Jiayin Tang, Junping Luo, Xianfeng Wu, Ruilin Mao, Wenjing Xu, Guangdi Zhou, Zhengang Dong, Bohan Feng, Lingchi Shi, Zhicheng Pei, Peng Gao, Zhuoyu Chen, and Danfeng Li, "Enhanced superconductivity in co-doped infinite-layer samarium nickelate thin films," *arXiv preprint arXiv:2503.18346* (2025).

[38] C. T. Parzyck, Y. Wu, L. Bhatt, M. Kang, Z. Arthur, T. M. Pedersen, R. Sutarto, S. Fan, J. Pelliciari, V. Bisogni, G. Herranz, A. B. Georgescu, D. G. Hawthorn, L. F. Kourkoutis, D. A. Muller, D. G. Schlom, and K. M. Shen, "Superconductivity in the Parent Infinite-Layer Nickelate NdNiO_2 ," *Phys. Rev. X* **15**, 021048 (2025).

[39] Hoshang Sahib, Aravind Raji, Francesco Rosa, Giacomo Merzoni, Giacomo Ghiringhelli, Marco Salluzzo, Alexandre Gloter, Nathalie Viart, and Daniele Preziosi, "Superconductivity in PrNiO_2 infinite-layer nickelates," *Advanced Materials* **37**, 2416187 (2025).

[40] Zhengang Dong, Marios Hadjimichael, Bernat Mundet, Jaewon Choi, Charles C. Tam, Mirian Garcia-Fernandez, Stefano Agrestini, Claribel Domínguez, Regan Bhatta, Yue Yu, Yufeng Liang, Zhenping Wu, Jean-Marc Triscone, Chunjing Jia, Ke-Jin Zhou, and Danfeng Li, "Topochemical synthesis and electronic structure of high-crystallinity infinite-layer nickelates on an orthorhombic substrate," *Nano Letters* **25**, 1233–1241 (2025).

[41] J. Zaanen, G. A. Sawatzky, and J. W. Allen, "Band gaps and electronic structure of transition-metal compounds," *Phys. Rev. Lett.* **55**, 418–421 (1985).

[42] Mi Jiang, Mona Berciu, and George A. Sawatzky, "Critical Nature of the Ni Spin State in Doped NdNiO_2 ," *Phys. Rev. Lett.* **124**, 207004 (2020).

[43] Wenjie Sun, Zhicheng Jiang, Chengliang Xia, Bo Hao, Shengjun Yan, Maosen Wang, Yueying Li, Hongquan Liu, Jianyang Ding, Jiayu Liu, Zhengtai Liu, Jishan Liu, Hanghui Chen, Dawei Shen, and Yuefeng Nie, "Electronic structure of superconducting infinite-layer lanthanum nickelates," *Science Advances* **11**, eadrf5116 (2025).

[44] Xiang Ding, Yu Fan, Xiaoxiao Wang, Chihao Li, Zhitong An, Jiahao Ye, Shenglin Tang, Minyan Lei, Xingtian Sun, Nan Guo, Zhihui Chen, Suppanut Sangphet, Yilin Wang, Haichao Xu, Rui Peng, and Donglai Feng, “Cuprate-like electronic structures in infinite-layer nickelates with substantial hole dopings,” *National Science Review* **11**, nwae194 (2024).

[45] Ziyan Chen, Yuxin Wang, Kun Jiang, and Jiangping Hu, “Electronic structure and superconducting properties of LaNiO_2 ,” *arXiv preprint arXiv:2411.03777* (2024).

[46] Guang-Ming Zhang, Yi-feng Yang, and Fu-Chun Zhang, “Self-doped mott insulator for parent compounds of nickelate superconductors,” *Phys. Rev. B* **101**, 020501 (2020).

[47] Kyuho Lee, Bai Yang Wang, Motoki Osada, Berit H. Goodge, Tiffany C. Wang, Yonghun Lee, Shannon Harvey, Woo Jin Kim, Yijun Yu, Chaitanya Murthy, Srinivas Raghu, Lena F. Kourkoutis, and Harold Y. Hwang, “Linear-in-temperature resistivity for optimally superconducting $(\text{Nd},\text{Sr})\text{NiO}_2$,” *Nature* **619**, 288–292 (2023).

[48] Motoki Osada, Bai Yang Wang, Berit H. Goodge, Shannon P. Harvey, Kyuho Lee, Danfeng Li, Lena F. Kourkoutis, and Harold Y. Hwang, “Nickelate superconductivity without rare-earth magnetism: $(\text{La}, \text{Sr})\text{NiO}_2$,” *Advanced Materials* **33**, 2104083 (2021).

[49] Yanan Zhang, Dajun Su, Yanen Huang, ZhaoYang Shan, Hualei Sun, Mengwu Huo, Kaixin Ye, Jiawen Zhang, Zihan Yang, Yongkang Xu, Yi Su, Rui Li, Michael Smidman, Meng Wang, Lin Jiao, and Huiqiu Yuan, “High-temperature superconductivity with zero resistance and strange-metal behaviour in $\text{La}_3\text{Ni}_2\text{O}_{7-\delta}$,” *Nature Physics* **20**, 1269–1273 (2024).

[50] Shannon P. Harvey, Bai Yang Wang, Jennifer Fowlie, Motoki Osada, Kyuho Lee, Yonghun Lee, Danfeng Li, and Harold Y. Hwang, “Evidence for nodal superconductivity in infinite-layer nickelates,” *arXiv preprint arXiv:2201.12971* (2022).

[51] L. E. Chow, S. Kunniniyil Sudheesh, Z. Y. Luo, P. Nandi, T. Heil, J. Deuschle, S. W. Zeng, Z. T. Zhang, S. Prakash, X. M. Du, Z. S. Lim, Peter A. van Aken, Elbert E. M. Chia, and A. Ariando, “Pairing symmetry in infinite-layer nickelate superconductor,” *arXiv preprint arXiv:2201.10038* (2022).

[52] G. Grissonnanche, G. A. Pan, H. LaBollita, D. Ferenc Segedin, Q. Song, H. Paik, C. M. Brooks, E. Beauchesne-Blanchet, J. L. Santana González, A. S. Botana, J. A. Mundy, and B. J. Ramshaw, “Electronic band structure of a superconducting nickelate probed by the seebeck coefficient in the disordered limit,” *Phys. Rev. X* **14**, 041021 (2024).

[53] Bing Cheng, Di Cheng, Kyuho Lee, Liang Luo, Zhuoyu Chen, Yonghun Lee, Bai Yang Wang, Martin Mootz, Ilias E. Perakis, Zhi-Xun Shen, Harold Y. Hwang, and Jigang Wang, “Evidence for d -wave superconductivity of infinite-layer nickelates from low-energy electrodynamics,” *Nature Materials* **23**, 775–781 (2024).

[54] Abhishek Ranna, Romain Grasset, Martin Gonzalez, Kyuho Lee, Bai Yang Wang, Edgar Abarca Morales, Florian Theuss, Zuzanna H. Filipiak, Michal Moravec, Marcin Konczykowski, Harold Y. Hwang, Andrew P. Mackenzie, and Berit H. Goodge, “Disorder-induced suppression of superconductivity in infinite-layer nickelates,” *arXiv preprint arXiv:2506.09543* (2025).

[55] Meng Wang, Hai-Hu Wen, Tao Wu, Dao-Xin Yao, and Tao Xiang, “Normal and Superconducting Properties of $\text{La}_3\text{Ni}_2\text{O}_7$,” *Chinese Physics Letters* **41**, 077402 (2024).

[56] Jingyuan Li, Di Peng, Peiyue Ma, Hengyuan Zhang, Zhenfang Xing, Xing Huang, Chaoxin Huang, Mengwu Huo, Deyuan Hu, Zixian Dong, *et al.*, “Identification of superconductivity in bilayer nickelate $\text{La}_3\text{Ni}_2\text{O}_7$ under high pressure up to 100 GPa,” *National Science Review*, nwaf220 (2025).

[57] Yazhou Zhou, Jing Guo, Shu Cai, Hualei Sun, Chengyu Li, Jinyu Zhao, Pengyu Wang, Jinyu Han, Xintian Chen, Yongjin Chen, Qi Wu, Yang Ding, Tao Xiang, Ho-kwang Mao, and Liling Sun, “Investigations of key issues on the reproducibility of high-Tc superconductivity emerging from compressed $\text{La}_3\text{Ni}_2\text{O}_7$,” *Matter and Radiation at Extremes* **10**, 027801 (2025).

[58] P. Puphal, P. Reiss, N. Enderlein, Y.-M. Wu, G. Khalilullin, V. Sundaramurthy, T. Priessnitz, M. Knauff, A. Suthar, L. Richter, M. Isobe, P. A. van Aken, H. Takagi, B. Keimer, Y. E. Suyolcu, B. Wehinger, P. Hansmann, and M. Hepting, “Unconventional Crystal Structure of the High-Pressure Superconductor $\text{La}_3\text{Ni}_2\text{O}_7$,” *Phys. Rev. Lett.* **133**, 146002 (2024).

[59] Zengjia Liu, Hualei Sun, Mengwu Huo, Xiaoyan Ma, Yi Ji, Enkui Yi, Lisi Li, Hui Liu, Jia Yu, Ziyou Zhang, Zhiqiang Chen, Feixiang Liang, Hongliang Dong, Hanjie Guo, Dingyong Zhong, Bing Shen, Shiliang Li, and Meng Wang, “Evidence for charge and spin density waves in single crystals of $\text{La}_3\text{Ni}_2\text{O}_7$ and $\text{La}_3\text{Ni}_2\text{O}_6$,” *Science China Physics, Mechanics & Astronomy* **66**, 217411 (2022).

[60] Kaiwen Chen, Xiangqi Liu, Jiachen Jiao, Muyuan Zou, Chengyu Jiang, Xin Li, Yixuan Luo, Qiong Wu, Ningyuan Zhang, Yanfeng Guo, and Lei Shu, “Evidence of Spin Density Waves in $\text{La}_3\text{Ni}_2\text{O}_{7-\delta}$,” *Phys. Rev. Lett.* **132**, 256503 (2024).

[61] Xiaoyang Chen, Jaewon Choi, Zhicheng Jiang, Jiong Mei, Kun Jiang, Jie Li, Stefano Agrestini, Mirian Garcia-Fernandez, Hualei Sun, Xing Huang, Dawei Shen, Meng Wang, Jiangping Hu, Yi Lu, Ke-Jin Zhou, and Donglai Feng, “Electronic and magnetic excitations in $\text{La}_3\text{Ni}_2\text{O}_7$,” *Nature Communications* **15**, 9597 (2024).

[62] Dan Zhao, Yanbing Zhou, Mengwu Huo, Yu Wang, Linpeng Nie, Ye Yang, Jianjun Ying, Meng Wang, Tao Wu, and Xianhui Chen, “Pressure-enhanced spin-density-wave transition in double-layer nickelate $\text{La}_3\text{Ni}_2\text{O}_{7-\delta}$,” *Science Bulletin* **70**, 1239–1245 (2025).

[63] Igor Plokhikh, Thomas J. Hicken, Lukas Keller, Vladimir Pomjakushin, Samuel H. Moody, Pascale Foury-Leylekian, Jonas J. Krieger, Hubertus Luetkens, Zurab Guguchia, Rustem Khasanov, and Dariusz Jakub Gawryluk, “Unraveling Spin Density Wave Order in Layered Nickelates $\text{La}_3\text{Ni}_2\text{O}_7$ and $\text{La}_2\text{PrNi}_2\text{O}_7$ via Neutron Diffraction,” *arXiv preprint arXiv:2503.05287* (2025).

[64] G. Wang, N. N. Wang, X. L. Shen, J. Hou, L. Ma, L. F. Shi, Z. A. Ren, Y. D. Gu, H. M. Ma, P. T. Yang, Z. Y. Liu, H. Z. Guo, J. P. Sun, G. M. Zhang, S. Calder, J.-Q. Yan, B. S. Wang, Y. Uwatoko, and J.-G. Cheng, “Pressure-Induced Superconductivity In Polycrystalline $\text{La}_3\text{Ni}_2\text{O}_{7-\delta}$,” *Phys. Rev. X* **14**, 011040 (2024).

[65] Eun Kyo Ko, Yijun Yu, Yidi Liu, Lopa Bhatt, Jiarui Li, Vivek Thampy, Cheng-Tai Kuo, Bai Yang Wang, Yonghun Lee, Kyuho Lee, *et al.*, “Signatures of ambient pressure superconductivity in thin film $\text{La}_3\text{Ni}_2\text{O}_7$,” *Nature (London)* **638** (2024).

[66] Zhihui Luo, Xunwu Hu, Meng Wang, Wéi Wú, and Dao-Xin Yao, “Bilayer Two-Orbital Model of $\text{La}_3\text{Ni}_2\text{O}_7$ under Pressure,” *Phys. Rev. Lett.* **131**, 126001 (2023).

[67] Yuxin Wang, Kun Jiang, Ziqiang Wang, Fu-Chun Zhang, and Jiangping Hu, “Electronic and magnetic structures of bilayer $\text{La}_3\text{Ni}_2\text{O}_7$ at ambient pressure,” *Phys. Rev. B* **110**, 205122 (2024).

[68] Yuxin Wang, Yi Zhang, and Kun Jiang, “Electronic structure and disorder effect of $\text{La}_3\text{Ni}_2\text{O}_7$ superconductor,” *Chinese Physics B* **34**, 047105 (2025).

[69] Zehao Dong, Mengwu Huo, Jie Li, Jingyuan Li, Pengcheng Li, Hualei Sun, Lin Gu, Yi Lu, Meng Wang, Yayu Wang, and Zhen Chen, “Visualization of oxygen vacancies and self-doped ligand holes in $\text{La}_3\text{Ni}_2\text{O}_{7-\delta}$,” *Nature* **630**, 847–852 (2024).

[70] Jiangang Yang, Hualei Sun, Xunwu Hu, Yuyang Xie, Taimin Miao, Hailan Luo, Hao Chen, Bo Liang, Wenpei Zhu, Gexing Qu, *et al.*, “Orbital-dependent electron correlation in double-layer nickelate $\text{La}_3\text{Ni}_2\text{O}_7$,” *Nature Communications* **15**, 4373 (2024).

[71] Masataka Kakoi, Takashi Oi, Yujiro Ohshita, Mitsuharu Yashima, Kazuhiko Kuroki, Takeru Kato, Hidefumi Takahashi, Shintaro Ishiwata, Yoshinobu Adachi, Naoyuki Hatada, Tetsuya Uda, and Hidekazu Mukuda, “Multiband Metallic Ground State in Multilayered Nickelates $\text{La}_3\text{Ni}_2\text{O}_7$ and $\text{La}_4\text{Ni}_3\text{O}_{10}$ Probed by ^{139}La -NMR at Ambient Pressure,” *Journal of the Physical Society of Japan* **93**, 053702 (2024).

[72] T Fukamachi, Y Kobayashi, T Miyashita, and M Sato, “ ^{139}La NMR studies of layered perovskite systems $\text{La}_3\text{Ni}_2\text{O}_{7-\delta}$ and $\text{La}_4\text{Ni}_3\text{O}_{10}$,” *Journal of Physics and Chemistry of Solids* **62**, 195–198 (2001).

[73] Toshihiko Fukamachi, Keisuke Oda, Yoshiaki Kobayashi, Takeshi Miyashita, and Masatoshi Sato, “Studies on Successive Electronic State Changes in Systems with NiO_2 Planes- ^{139}La -NMR/NQR,” *Journal of the Physical Society of Japan* **70**, 2757–2764 (2001).

[74] Rustem Khasanov, Thomas J Hicken, Dariusz J Gawryluk, Vahid Sazgari, Igor Plokhikh, Loic Pierre Sorel, Marek Bartkowiak, Steffen Böttzel, Frank Lechermann, Ilya M Eremin, *et al.*, “Pressure-enhanced splitting of density wave transitions in $\text{La}_3\text{Ni}_2\text{O}_{7-\delta}$,” *Nature Physics*, 1–7 (2025).

[75] Zhe Liu, Mengwu Huo, Jie Li, Qing Li, Yuecong Liu, Yaomin Dai, Xiaoxiang Zhou, Jiahao Hao, Yi Lu, Meng Wang, *et al.*, “Electronic correlations and partial gap in the bilayer nickelate $\text{La}_3\text{Ni}_2\text{O}_7$,” *Nature Communications* **15**, 7570 (2024).

[76] Mitsuharu Yashima, Nina Seto, Yujiro Oshita, Masataka Kakoi, Hiroya Sakurai, Yoshihiko Takano, and Hidekazu Mukuda, “Microscopic evidence for spin-spinless stripe order with reduced Ni moments within ab plane for bilayer nickelate $\text{La}_3\text{Ni}_2\text{O}_7$ probed by ^{139}La -NQR,” *Journal of the Physical Society of Japan* **94**, 054704 (2025).

[77] J. Luo, J. Feng, G. Wang, N. N. Wang, J. Dou, A. F. Fang, J. Yang, J. G. Cheng, Guo-qing Zheng, and R. Zhou, “Microscopic evidence of charge- and spin-density waves in $\text{La}_3\text{Ni}_2\text{O}_{7-\delta}$ revealed by ^{139}La -NQR,” *Chin. Phys. Lett.* (2025).

[78] Ting Cui, Songhee Choi, Ting Lin, Chen Liu, Gang Wang, Ningning Wang, Shengru Chen, Haitao Hong, Dongke Rong, Qianying Wang, Qiao Jin, Jia-Ou Wang, Lin Gu, Chen Ge, Can Wang, Jin-Guang Cheng, Qinghua Zhang, Liang Si, Kuijuan Jin, and Er-Jia Guo, “Strain-mediated phase crossover in ruddlesden–popper nickelates,” *Communications Materials* **5**, 32 (2024).

[79] Guangdi Zhou, Wei Lv, Heng Wang, Zihao Nie, Yaqi Chen, Yueying Li, Haoliang Huang, Weiqiang Chen, Yujie Sun, Qi-Kun Xue, and Zhuoyu Chen, “Ambient-pressure superconductivity onset above 40 K in bilayer nickelate ultrathin films,” *arXiv preprint arXiv:2412.16622* (2024).

[80] Yidi Liu, Eun Kyo Ko, Yaoju Tarn, Lopa Bhatt, Berit H. Goodge, David A. Muller, Srinivas Raghu, Yijun Yu, and Harold Y. Hwang, “Superconductivity and normal-state transport in compressively strained $\text{La}_2\text{PrNi}_2\text{O}_7$ thin films,” *arXiv preprint arXiv:2501.08022* (2025).

[81] Bo Hao, Maosen Wang, Wenjie Sun, Yang Yang, Zhangwen Mao, Shengjun Yan, Haoying Sun, Hongyi Zhang, Lu Han, Zhengbin Gu, Jian Zhou, Dianxiang Ji, and Yuefeng Nie, “Superconductivity and phase diagram in Sr-doped $\text{La}_{3-x}\text{Sr}_x\text{Ni}_2\text{O}_7$ thin films,” *arXiv preprint arXiv:2505.12603* (2025).

[82] Baiyang Wang, Yong Zhong, Sebastien Abadi, Yidi Liu, Yijun Yu, Xiaoliang Zhang, Yi-Ming Wu, Ruohan Wang, Jiarui Li, Yaoju Tarn, Eun Kyo Ko, Vivek Thampy, Makoto Hashimoto, Donghui Lu, Young S. Lee, Thomas P. Devereaux, Chunjing Jia, Harold Y. Hwang, and Zhi-Xun Shen, “Electronic structure of compressively strained thin film $\text{La}_2\text{PrNi}_2\text{O}_7$,” *arXiv preprint arXiv:2504.16372* (2025).

[83] Lopa Bhatt, Abigail Y. Jiang, Eun Kyo Ko, Noah Schnitzer, Grace A. Pan, Dan Ferenc Segedin, Yidi Liu, Yijun Yu, Yi-Feng Zhao, Edgar Abarca Morales, Charles M. Brooks, Antia S. Botana, Harold Y. Hwang, Julia A. Mundy, David A. Muller, and Berit H. Goodge, “Resolving Structural Origins for Superconductivity in Strain-Engineered $\text{La}_3\text{Ni}_2\text{O}_7$ Thin Films,” *arXiv preprint arXiv:2501.08204* (2025).

[84] Peng Li, Guangdi Zhou, Wei Lv, Yueying Li, Changming Yue, Haoliang Huang, Lizhi Xu, Jianchang Shen, Yu Miao, Wenhua Song, Zihao Nie, Yaqi Chen, Heng Wang, Weiqiang Chen, Yaobo Huang, Zhen-Hua Chen, Tian Qian, Junhao Lin, Junfeng He, Yu-Jie Sun, Zhuoyu Chen, and Qi-Kun Xue, “Angle-resolved photoemission spectroscopy of superconducting $(\text{La},\text{Pr})_3\text{Ni}_2\text{O}_7/\text{SrLaAlO}_4$ heterostructures,” *National Science Review*, nwaf205 (2025).

[85] Yu-Te Hsu, Yidi Liu, Yoshimitsu Kohama, Tommy Kotte, Vikash Sharma, Yaoju Tarn, Yijun Yu, and Harold Y. Hwang, “Fermi-liquid transport beyond the upper critical field in superconducting $\text{La}_2\text{PrNi}_2\text{O}_7$ thin films,” *arXiv preprint arXiv:2505.19011* (2025).

[86] Motoki Osada, Chieko Terakura, Akiko Kikkawa, Masamichi Nakajima, Hsiao-Yi Chen, Yusuke Nomura, Yoshinori Tokura, and Atsushi Tsukazaki, “Strain-tuning for superconductivity in $\text{La}_3\text{Ni}_2\text{O}_7$ thin films,” *Communications Physics* **8**, 251 (2025).

[87] Junjie Zhang, Daniel Phelan, A. S. Botana, Yu-Sheng Chen, Hong Zheng, M. Krogstad, Suyin Grass Wang, Yiming Qiu, J. A. Rodriguez-Rivera, and R. Osborn, “Intertwined density waves in a metallic nickelate,” *Nature communications* **11**, 6003 (2020).

[88] Jianchang Shen, Yu Miao, Zhipeng Ou, Guangdi Zhou, Yaqi Chen, Runqing Luan, Hongxu Sun, Zikun Feng, Xinru Yong, Peng Li, Yueying Li, Lizhi Xu, Wei Lv, Zihao Nie, Heng Wang, Haoliang Huang, Yu-Jie Sun, Qi-Kun Xue, Zhuoyu Chen, and Junfeng He, “Anomalous energy gap in superconducting $\text{La}_{2.85}\text{Pr}_{0.15}\text{Ni}_2\text{O}_7/\text{SrLaAlO}_4$ heterostructures,” *arXiv preprint arXiv:2502.17831* (2025).

[89] Yu-Bo Liu, Jia-Wei Mei, Fei Ye, Wei-Qiang Chen, and Fan Yang, “ s^\pm -Wave Pairing and the Destructive Role of Apical-Oxygen Deficiencies in $\text{La}_3\text{Ni}_2\text{O}_7$ under Pressure,” *Phys. Rev. Lett.* **131**, 236002 (2023).

[90] Yang Zhang, Ling-Fang Lin, Adriana Moreo, and Elbio Dagotto, “Electronic structure, dimer physics, orbital-selective behavior, and magnetic tendencies in the bilayer nickelate superconductor $\text{La}_3\text{Ni}_2\text{O}_7$ under pressure,” *Phys. Rev. B* **108**, L180510 (2023).

[91] Yang Zhang, Ling-Fang Lin, Adriana Moreo, Thomas A Maier, and Elbio Dagotto, “Trends in electronic structures and s^\pm -wave pairing for the rare-earth series in bilayer nickelate superconductor $\text{R}_3\text{Ni}_2\text{O}_7$,” *Physical Review B* **108**, 165141 (2023).

[92] Frank Lechermann, Jannik Gondolf, Steffen Böttzel, and

Ilya M. Eremin, "Electronic correlations and superconducting instability in $\text{La}_3\text{Ni}_2\text{O}_7$ under high pressure," *Phys. Rev. B* **108**, L201121 (2023).

[93] Griffin Heier, Kyungwha Park, and Sergey Y Savrasov, "Competing d_{xy} and s^\pm pairing symmetries in superconducting $\text{La}_3\text{Ni}_2\text{O}_7$: LDA+ FLEX calculations," *Physical Review B* **109**, 104508 (2024).

[94] Yuhao Gu, Congcong Le, Zhesen Yang, Xianxin Wu, and Jiangping Hu, "Effective model and pairing tendency in the bilayer Ni-based superconductor $\text{La}_3\text{Ni}_2\text{O}_7$," *Physical Review B* **111**, 174506 (2025).

[95] Chengliang Xia, Hongquan Liu, Shengjie Zhou, and Hanghui Chen, "Sensitive dependence of pairing symmetry on Ni_{eg} crystal field splitting in the nickelate superconductor $\text{La}_3\text{Ni}_2\text{O}_7$," *Nature Communications* **16**, 1054 (2025).

[96] Wenhan Xi, Shun-Li Yu, and Jian-Xin Li, "Transition from $s\pm$ -wave to $d_{x^2-y^2}$ -wave superconductivity driven by interlayer interaction in the bilayer two-orbital model of $\text{La}_3\text{Ni}_2\text{O}_7$," *Physical Review B* **111**, 104505 (2025).

[97] Hirofumi Sakakibara, Naoya Kitamine, Masayuki Ochi, and Kazuhiko Kuroki, "Possible High T_c Superconductivity in $\text{La}_3\text{Ni}_2\text{O}_7$ under High Pressure through Manifestation of a Nearly Half-Filled Bilayer Hubbard Model," *Phys. Rev. Lett.* **132**, 106002 (2024).

[98] Steffen Böttzel, Frank Lechermann, Jannik Gondolf, and Ilya M. Eremin, "Theory of magnetic excitations in the multi-layer nickelate superconductor $\text{La}_3\text{Ni}_2\text{O}_7$," *Phys. Rev. B* **109**, L180502 (2024).

[99] Qing-Geng Yang, Da Wang, and Qiang-Hua Wang, "Possible s_\pm -wave superconductivity in $\text{La}_3\text{Ni}_2\text{O}_7$," *Phys. Rev. B* **108**, L140505 (2023).

[100] Kai-Yue Jiang, Yu-Han Cao, Qing-Geng Yang, Hong-Yan Lu, and Qiang-Hua Wang, "Theory of pressure dependence of superconductivity in bilayer nickelate $\text{La}_3\text{Ni}_2\text{O}_7$," *Physical Review Letters* **134**, 076001 (2025).

[101] Jun Zhan, Yuhao Gu, Xianxin Wu, and Jiangping Hu, "Cooperation between electron-phonon coupling and electronic interaction in bilayer nickelates $\text{La}_3\text{Ni}_2\text{O}_7$," *Physical Review Letters* **134**, 136002 (2025).

[102] Kun Jiang, Ziqiang Wang, and Fu-Chun Zhang, "High-temperature superconductivity in $\text{La}_3\text{Ni}_2\text{O}_7$," *Chinese Physics Letters* **41**, 017402 (2024).

[103] Zhen Fan, Jian-Feng Zhang, Bo Zhan, Dingshun Lv, Xing-Yu Jiang, Bruce Normand, and Tao Xiang, "Superconductivity in nickelate and cuprate superconductors with strong bilayer coupling," *Phys. Rev. B* **110**, 024514 (2024).

[104] Shen Yang *et al.*, "Effective Bi-Layer Model Hamiltonian and Density-Matrix Renormalization Group Study for the High- T_c Superconductivity in $\text{La}_3\text{Ni}_2\text{O}_7$ under High Pressure," *Chinese Physics Letters* **40**, 127401 (2023).

[105] Chen Lu, Zhiming Pan, Fan Yang, and Congjun Wu, "Interlayer-Coupling-Driven High-Temperature Superconductivity in $\text{La}_3\text{Ni}_2\text{O}_7$ under Pressure," *Phys. Rev. Lett.* **132**, 146002 (2024).

[106] Yi-feng Yang, Guang-Ming Zhang, and Fu-Chun Zhang, "Interlayer valence bonds and two-component theory for high- T_c superconductivity of $\text{La}_3\text{Ni}_2\text{O}_7$ under pressure," *Phys. Rev. B* **108**, L201108 (2023).

[107] Qiong Qin and Yi-feng Yang, "High- T_c superconductivity by mobilizing local spin singlets and possible route to higher T_c in pressurized $\text{La}_3\text{Ni}_2\text{O}_7$," *Physical Review B* **108**, L140504 (2023).

[108] Zhiguang Liao, Lei Chen, Guijing Duan, Yiming Wang, Changle Liu, Rong Yu, and Qimiao Si, "Electron correlations and superconductivity in $\text{La}_3\text{Ni}_2\text{O}_7$ under pressure tuning," *Physical Review B* **108**, 214522 (2023).

[109] Xing-Zhou Qu, Dai-Wei Qu, Jialin Chen, Congjun Wu, Fan Yang, Wei Li, and Gang Su, "Bilayer t - J - J_\perp model and magnetically mediated pairing in the pressurized nickelate $\text{La}_3\text{Ni}_2\text{O}_7$," *Physical Review Letters* **132**, 036502 (2024).

[110] Yi-Heng Tian, Yin Chen, Jia-Ming Wang, Rong-Qiang He, and Zhong-Yi Lu, "Correlation effects and concomitant two-orbital s^\pm -wave superconductivity in $\text{La}_3\text{Ni}_2\text{O}_7$ under high pressure," *Physical Review B* **109**, 165154 (2024).

[111] Zhihui Luo, Biao Lv, Meng Wang, Wéi Wú, and Dao-Xin Yao, "High- T_c superconductivity in $\text{La}_3\text{Ni}_2\text{O}_7$ based on the bilayer two-orbital t - J model," *npj Quantum Materials* **9**, 61 (2024).

[112] Zhan Wang, Heng-Jia Zhang, Kun Jiang, and Fu-Chun Zhang, "Self-doped molecular Mott insulator for bilayer high-temperature superconducting $\text{La}_3\text{Ni}_2\text{O}_7$," *arXiv preprint arXiv:2412.18469* (2024).

[113] Yao-Yuan Zheng and Wéi Wú, " s^\pm -wave superconductivity in the bilayer two-orbital Hubbard model," *Physical Review B* **111**, 035108 (2025).

[114] Mingzhe Li, Jiashuo Gong, Yinghao Zhu, Ziyuan Chen, Jiakang Zhang, Enkang Zhang, Yuanji Li, Ruotong Yin, Shiyuan Wang, Jun Zhao, Dong-Lai Feng, Zengyi Du, and Ya-Jun Yan, "Direct Visualization of an Incommensurate Unidirectional Charge Density Wave in $\text{La}_4\text{Ni}_3\text{O}_{10}$," *arXiv preprint arXiv:2501.18885* (2025).

[115] Yantao Cao, Andi Liu, Bin Wang, Mingxin Zhang, Yanpeng Qi, Thomas J Hicken, Hubertus Luetkens, Zhen-dong Fu, Jason S Gardner, Jinkui Zhao, *et al.*, "Complex spin-density-wave ordering in $\text{La}_4\text{Ni}_3\text{O}_{10}$," *arXiv preprint arXiv:2503.14128* (2025).

[116] Rustem Khasanov, Thomas J. Hicken, Igor Plokhikh, Vahid Sazgari, Lukas Keller, Vladimir Pomjakushin, Marek Bartkowiak, Szymon Królak, Michał J. Winiarski, Jonas A. Krieger, Hubertus Luetkens, Tomasz Klimczuk, Dariusz J. Gawryluk, and Zurab Guguchia, "Identical Suppression of Spin and Charge Density Wave Transitions in $\text{La}_4\text{Ni}_3\text{O}_{10}$ by Pressure," *arXiv preprint arXiv:2503.04400* (2025).

[117] Haoxiang Li, Xiaoqing Zhou, Thomas Nummy, Junjie Zhang, Victor Pardo, Warren E. Pickett, John F. Mitchell, and Dan S. Dessau, "Fermiology and electron dynamics of trilayer nickelate $\text{La}_4\text{Ni}_3\text{O}_{10}$," *Nature communications* **8**, 704 (2017).

[118] Yidian Li, Yantao Cao, Liangyang Liu, Pai Peng, Hao Lin, Cuiying Pei, Mingxin Zhang, Heng Wu, Xian Du, Wenxuan Zhao, Kaiyi Zhai, Xuefeng Zhang, Jinkui Zhao, Miaoling Lin, Pingheng Tan, Yanpeng Qi, Gang Li, Hanjie Guo, Luyi Yang, and Lexian Yang, "Distinct ultrafast dynamics of bilayer and trilayer nickelate superconductors regarding the density-wave-like transitions," *Science Bulletin* **70**, 180–186 (2025).

[119] X. Du, Y. D. Li, Y. T. Cao, C. Y. Pei, M. X. Zhang, W. X. Zhao, K. Y. Zhai, R. Z. Xu, Z. K. Liu, Z. W. Li, J. K. Zhao, G. II, Y. L. Chen, Y. P. Qi, and L. X. Yang, "Correlated Electronic Structure and Density-Wave Gap in Trilayer Nickelate $\text{La}_4\text{Ni}_3\text{O}_{10}$," *arXiv preprint arXiv:2405.19853* (2024).

[120] Shuxiang Xu, Cui-Qun Chen, Mengwu Huo, Deyuan Hu, Hao Wang, Qiong Wu, Rongsheng Li, Dong Wu, Meng Wang, Dao-Xin Yao, Tao Dong, and Nanlin Wang, "Origin of the density wave instability in trilayer nickelate $\text{La}_4\text{Ni}_3\text{O}_{10}$ revealed by optical and ultrafast spectroscopy," *Physical Review B* **111**, 075140 (2025).

[121] Shuxiang Xu, Hao Wang, Mengwu Huo, Deyuan Hu, Qiong Wu, Li Yue, Dong Wu, Meng Wang, Tao Dong, and Nanlin Wang, "Collapse of density wave and emergence of super-

conductivity in pressurized- $\text{La}_4\text{Ni}_3\text{O}_{10}$ evidenced by ultrafast spectroscopy,” [arXiv preprint arXiv:2503.05176 \(2025\)](#).

[122] Sebastien Abadi, Ke-Jun Xu, Eder G. Lomeli, Pascal Puphal, Masahiko Isobe, Yong Zhong, Alexei V. Fedorov, Sung-Kwan Mo, Makoto Hashimoto, Dong-Hui Lu, Brian Moritz, Bernhard Keimer, Thomas P. Devereaux, Matthias Hepting, and Zhi-Xun Shen, “Electronic Structure of the Alternating Monolayer-Trilayer Phase of $\text{La}_3\text{Ni}_2\text{O}_7$,” [Phys. Rev. Lett. **134**, 126001 \(2025\)](#).

[123] Jiangping Hu, Congcong Le, and Xianxin Wu, “Predicting unconventional high-temperature superconductors in trigonal bipyramidal coordinations,” [Phys. Rev. X **5**, 041012 \(2015\)](#).

[124] Jiangping Hu, “Identifying the genes of unconventional high temperature superconductors,” [Science Bulletin **61**, 561 \(2016\)](#).